RICERCA DI SISTEMA ELETTRICO

Seismic risk computation for the base-isolated reactor building of the IRIS NPP

M. Domaneschi, F. Perotti

SEISMIC RISK COMPUTATION FOR THE BASE-ISOLATED REACTOR BUILDING OF THE IRIS NPP
M. Domaneschi, F. Perotti - POLIMI

Settembre 2011

POLITECNICO DI MILANO
DIPARTIMENTO DI INGEGNERIA STRUTTURALE

DIPARTIMENTO DI ENERGIA

SEISMIC RISK COMPUTATION FOR THE BASE-ISOLATED REACTOR BUILDING OF THE IRIS NPP

Autori

M. Domaneschi

F. Perotti

Milan September 2011

TABLE OF CONTENTS

1.   Introduction

This report deals with the fragility assessment of the IRIS reactor building in its base-isolated version, following the previous configuration without any isolation system [1]. The aim of this step consists in the evaluation of the effectiveness of the base-isolation when applied to the IRIS NPP for the reduction of the seismic risk and in the comparison between the performance of the traditional and the isolated reactor building. Since the behavior of the isolators is markedly hysteretic, the hypothesis of linearity of the building response, typical of the traditional building, has been removed herein, and a suitable force-displacement literature model is adopted to represent the isolators inelastic response to horizontal loading.

The probabilistic assessment is based on the procedure described in [2], on a nonlinear analytical model, by performing sequential seismic analyses in the MATLAB framework [3], with the application of an explicit direct integration method. Previous studies [4] on an extensive finite element model of the isolated IRIS reactor building allow to introduce the rigid body condition for the structural equation of motion.

The most important requirement of the procedure remains to reduce as much as possible the uncertainties related to the incomplete knowledge and accuracy in defining models and methods; this reduction is here sought by refining analysis procedures and using consolidated analytical and numerical tools.

The characterization of the isolator devices has been preliminarily performed by testing scaled prototypes, in view of further full scale laboratory experimentations; the definition of the limit state domain for the reference device in terms of the total vertical and horizontal forces has been also evaluated.

The definition of the random variables and the generation of the seismic excitations are also key aspects of the analysis. They represent significant requisites for setting up the probabilistic assessment of the response of the structural system.

The exceedance probability of the control system limit state domain is here computed via Monte Carlo simulations; to reduce the computational effort, the response surface (RS) method is used to express the seismic response as a function of the variation of the adopted random parameters. The generation of the RSs is performed in terms of mean and standard deviation of the minimum distance from a specific limit domain. In such setting, the RS evaluation must be repeated for every value of peak ground acceleration; on the other hand, to evaluate the isolators' behavior, the seismic behavior of the isolated building can be captured by means of a very simple mechanical model which can be based on the hypothesis of rigid-body motion of the building.

Finally, the results of the fragility analysis are computed, also in view of a refinement of the response surfaces, within a complete risk assessment for a prototype site.

2.   A literature review for a mathematical model of a base isolation system

Following the choice of implementing high damping rubber bearings (HDRB)for the IRIS NPP isolation system, a preliminary literature review has been developed for assessing the suitable numerical model. Some main features characterize the isolator devices are the strong nonlinear response, the *scragging* and *Mullins'* effects (stiffness and damping degradation), the horizontal stiffness variation (due to temperature and axial load), strain-rate dependence and ageing.

A first overview on this technology, including modeling and analysis options, can be found in the research report [5]. Even if it is oriented not specifically to NPP buildings, the report describes the main characteristics of a seismic isolation system, listing several models for the unidirectional numerical simulation. Finally, a bidirectional model is also proposed for representing the bearings response to bidirectional loading in terms of stiffness, damping and degradation. It consists in a decomposition of the bearing resisting force as the sum of elastic component (from Mooney-Rivlin strain energy function) and an hysteretic force.

Kikuchi and Aiken proposed a non-differential unidirectional model for elastomeric isolation bearings [6], developed from the Fujita one, in order to improve the performance into the large strain range. The Fujita model has the characteristic of including a procedure to update model parameters in contrary to other differential models as Ozdemir or Wen one. The proposed model neglects the effects of strain rate and variation of axial load on the bearing hysteresis.

Hwang et al [7] present a different analytical unidirectional model developed from a previous version by Pan and Yang for high damping elastomeric isolation devices. This model has been developed for describing the damping and the restoring force of a rubber material; the first component of the total resisting force is considered herein as a viscoelastic dissipation, that depends on the strain rate. The study investigates in particular the *Mullins'* and *scragging* effect, frequency and temperature dependence. Axial loads and rubber compounds are not considered. The model parameters identification is also not included in this study, which is mainly focused on the potential of the proposed approach in the prediction of the force-displacement hysteresis.

The differential unidirectional model for HDRB by Tsai et al [8] has been developed by modifying the Wen model to include rate-dependent effects under constant axial loads. The good correlation between experimental and numerical results does not show the stiffness and damping degradation, induced by *Mullins* and *scragging* effects, which is distinctive of such devices.

A nonlinear rate dependent unidirectional model for HDRB is proposed by Jankovsky in [9] under constant axial loads. It is a non-differential model developed from the Pan and Yang solution. The cyclic experimental tests are well reproduced by the model, even if it seems to loose its good performance when a seismic signal is applied.

Abe et al [10,11] propose differential hysteretic models of laminated rubber bearings (HDRB, rubber bearings (LRB), natural rubber bearings (NRB)) under biaxial and triaxial loading conditions on the basis of experimental results. Firstly, an unidirectional model is proposed by extending the Ozdemir elasto-plastic model; second, a bidirectional model of the bearing is derived. They result accurate in the simulation of the device response also under the seismic action.

The study proposed by Ryan et al [12] approaches the problem of the influence of the axial load variation in the isolator horizontal stiffness and yielding strength (in particular when the lead core is implemented or HDRB are considered). The following considerations has been underlined for both HDRB and lead LRB:

- the lateral stiffness decreases with the increasing axial load;
- the lateral yield strength decreases with decreasing axial load (LRB only);
- the vertical stiffness decreases with increasing lateral deformation.

Some considerations on the numerical modeling of HDRB and LRB devices are also included but the proposed solutions, although an improvement, are reported by the Authors as an incomplete representation of the experimental response.

Table 1. Main characteristics of the evaluated models

	Grant et al. [5]	Kikuchi et al. [6]	Hwang et al. [7]	Tsai et al. [8]	Jankovsky [9]
Dimension	Bidirectional	Unidirectional	Unidirectional	Unidirectional	Unidirectional
Formulation	Differential	Non-differential	Non-differential	Differential	Non-differential
Device	HDRB	LRB-HDRB	HDRB	HDRB	HDRB
Axial load	Constant	Constant	Constant	Constant	Constant
Modified version of	-	Fujita	Pan & Yang	Bouc-Wen	Pan & Yang
Degradation	Y	Y	Y	Y	Y
Hysteretic damping	Y	Y	N	Y	N
Viscoelastic damping	Y	N	Y	Y	Y
Rate-dependent effects	Y	N	Y	Y	Y
Temperature	N	N	Y	N	N
Parameters identification	Y	Y	N	Y	Y
Cyclic response	Y	Y	Y	Y	Y
Seismic response	N	Y	Y	N	N

	Abe et al. [10,11]	Ryan et al. [12]	Yamamoto et al. [13]	Kikuchi et al. [14]
Dimension	Uni & Bidirectional	Unidirectional	Unidirectional	Bidirectional (**)
Formulation	Differential	Non-differential	Non-differential	Non-differential
Device	NRB-LRB-HDRB	LRB-HDRB	LRB-HDRB	LRB-HDRB
Axial load	Constant	Variable (*)	Variable (*)	Variable (*)
Modified version of	Ozdemir	Kelly	Kikuchi & Aiken	Yamamoto et al. [13]
Degradation	Y	N	Y	Y
Hysteretic damping	Y	Y	Y	Y
Viscoelastic damping	N	N	N	N
Rate-dependent effects	N	N	N	N
Temperature	N	N	N	N
Parameters identification	Y	Y	Y	Y
Cyclic response	Y	N	Y	Y
Seismic response	Y	N	Y	N

(*   the model properties vary with the applied axial load)
(** three dimensional loading paths have not been evaluated)

The study by Yamamoto et al. [13] proposes a two-dimensional analytical model the numerical simulation of seismic isolation bearings including the influence of axial load. Such model is an

analytical mechanical model comprising shear and axial springs with properties varying with the vertical load. It has the advantage that the shear hysteresis used need not to incorporate the influence of axial load, since the influence of axial load on shear is implicitly captured by the material nonlinearity of the axial springs and the geometric nonlinearity in the model. A three dimensional development of this model has been reported in [14] but it lack of the evaluation under three dimensional loading paths (e.g. circular or "8" shapes in the horizontal plane) and also under seismic loads.

Table I reports the main characteristics of the evaluated models. The approach proposed by Abe et al. [10, 11] has been selected for the numerical simulations presented in the next sections for its versatility (uni and bidirectional application) and for the good representation of the experimental response for both the seismic and cyclic loading; also considering three dimensional loading paths in the horizontal plane. One feature lacking in this model could be found in the parameters definition as function of the axial load variation. It should be a further development, by including a updating time step procedure.

3.   The structural models of the base-isolated reactor building

IRIS (International Reactor Innovative and Secure) is a medium power (335 MWe) pressurized light water reactor under development by an international consortium which includes more than 20 partners from 10 countries (see [15]). Installation in a site characterized by a low-to-average seismicity level has been here assumed.

In a tentative design of the NSSS building (see Figure 1a), the introduction of an isolation system was considered; the system is made by High Damping Rubber Bearings (HDRB) installed between the foundation slab and the base (Figure 2b). The main scheme of the isolators layout, as considered in the preliminary design approach, is depicted in Figures 2c-d. The HDRB devices are made of alternated rubber layers and steel plates, bonded through vulcanization. Damping factor ranges from 10% to 20%, while shear modulus (G) lies in the 0.8-1.4 MPa range.

Steel plates give a high vertical stiffness to the isolator, though allowing large horizontal deformations. Therefore, the isolated building has low natural frequencies for motions lying in the horizontal plane, typically in the range 0.5 - 0.7 Hz, where the spectrum of ground motion has generally quite low energy. In such vibration modes the isolated building moves like a rigid body (see also [4]) over the isolators, which are strained in shear (continuously carrying the dead load). The absolute acceleration of the building can be much smaller than the PGA, with no amplification at higher floors. This is obtained at the price of large relative displacements between the building and the adjacent ground; this can be a problem for the design of the expansion joints and the connections with non isolated buildings of all the pipelines and service networks. The design of the isolation system, therefore, must reach a reasonable compromise between limitation of absolute accelerations and relative displacements. For the case of the IRIS NSSS, having a fixed-base first natural frequency of 5.91 Hz (on firm ground) and natural frequencies around 9 Hz for the vessel local motion, this led to a 0.7 Hz isolation frequency, i.e. to a value which can be seen as an upper limit for the parameter. If some equipment component (e.g., some wide span pipeline) has a lower natural frequency a local specific measure (stiffening or energy dissipation device) must be adopted.

The choice of 0.7 Hz as isolation frequency limits the relative displacement between the isolated building and the ground to 10 cm at the SSE level which is advantageous both for the performance of the isolators in beyond design conditions and for the design of steam lines connecting the NSSS building with the turbine units.

To compute the fragility of the IRIS isolation system, as detailed in following sections, the following aspects will be considered

• a first 3-DOFS vertical plane model has been adopted for the reactor building, under the hypothesis that the isolated superstructure behaves like a rigid body; soil-structure interaction has been neglected. Also a 6-DOFS 3D-model has been implemented, as a more general evaluation of the structural problem.

• The behavior of isolators under horizontal and vertical loading has been regarded as independent; it is assumed that isolators behave as linear elastic under vertical loading, showing the same stiffness in tension and compression. Their non linear behavior under horizontal loading has been modeled according to the uni and bidirectional models described in [11] respectively for the 3 and 6-DOFS reactor building simulation.
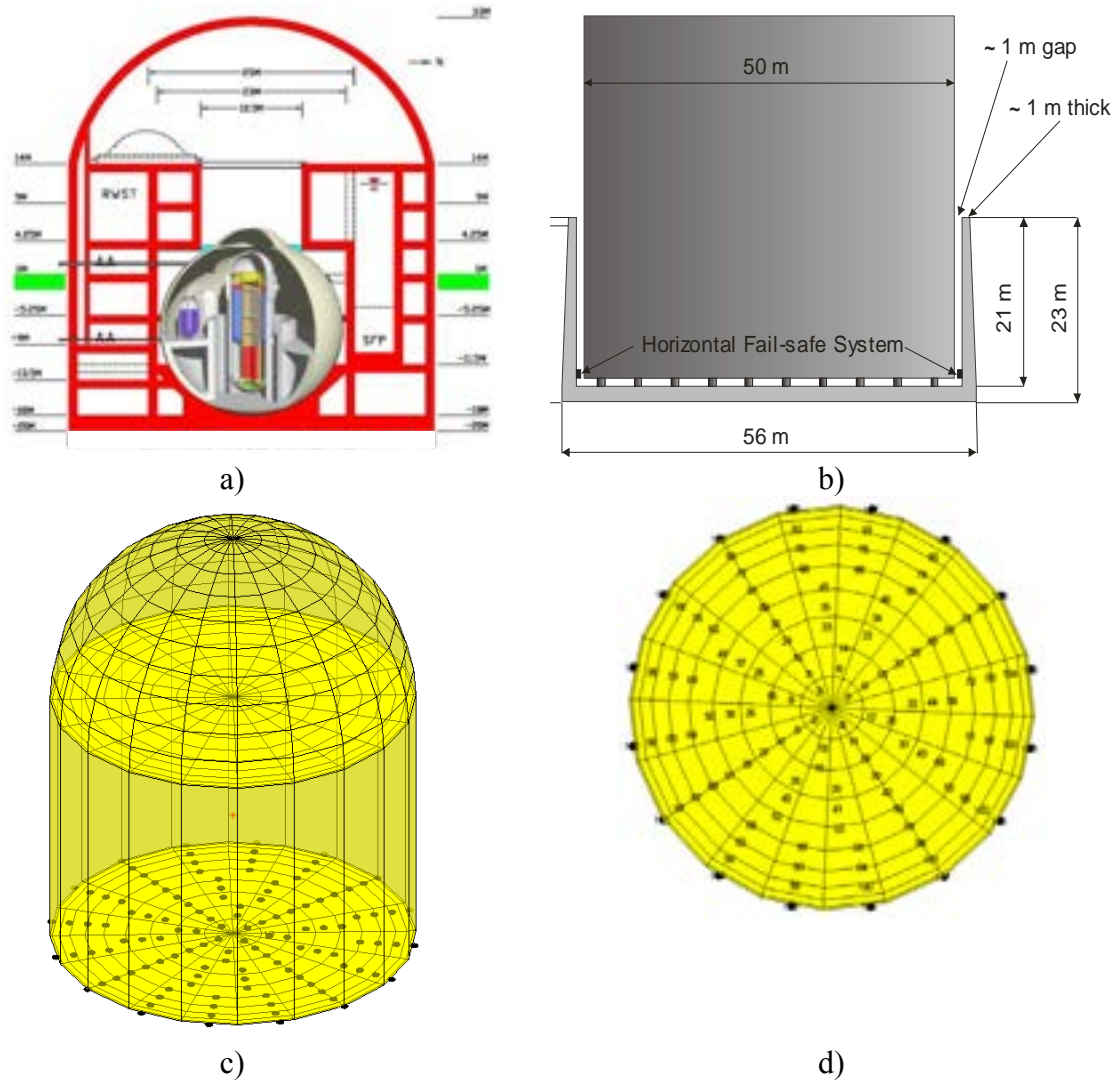

Figure 1. IRIS NSSS building (a); isolation system (b); isolators layout (c-d)

According to the unidirectional approach in [11] the restoring force for the HDRB device is the sum of three contributions, i.e. an elastic-plastic model (F_2 contribution) and two elastic non-linear springs, namely a non-linear elastic spring (F_1) and an hardening spring (F_3); the model allows to reproduce analytically some aspects of the experimental behavior of laminated rubber bearings. In light of these observations the resulting scheme for the Abe et al. [11] model is represented in Fig. 2a.
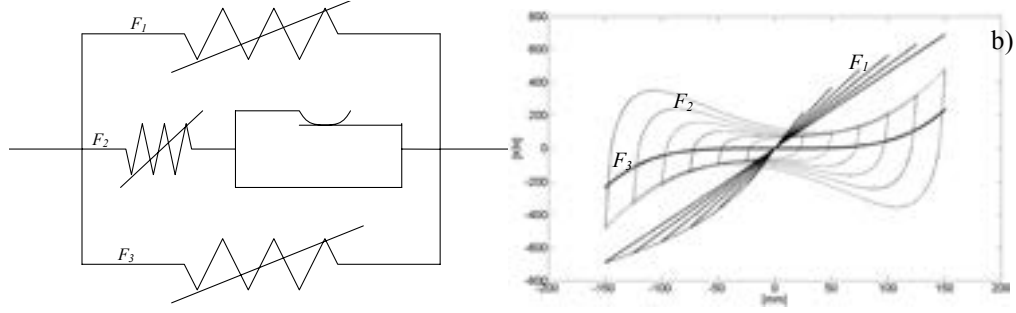
a)

Figure 2. Scheme of the HDRB model [11] (a); F_1, F_2, F_3 components under cyclic loading (b)

From an analytical point of view the force-displacement relation for the first non-linear spring consists of

$$F_1 = K_1 \left\{ \beta + (1-\beta) \exp(-\frac{U_{max}}{\alpha}) \right\} U + a \left[1 - \exp(-b|U|) \right] \operatorname{sgn}(U)$$

(1)

where U is the relative displacement and K_1, a e b parameters. In Equation (1), the first term reproduces the force linear evolution, while the second one the non-linear behavior. In Figure 2b the F_1 contribution is depicted for a cyclic experimental test on a reference specimen as force-displacement diagram up to displacement values equal to 300% of the rubber height. The stiffness degradation during the variable cycle amplitude is also highlighted by F_1.
The hysteretic contribution F_2 is described with a differential equation

$$\dot{F}_2 = \frac{Y_t}{U_t} \left\{ \dot{U} - |\dot{U}| \left| \frac{F_2}{Y_t} \right|^n \operatorname{sgn}(\frac{F_2}{Y_t}) \right\}$$

(2)

The values of Y_t and U_t are defined as

$$Y_t = Y_0 (1 + \left| \frac{U}{U_H} \right|^p) \quad ; \quad U_t = U_0 (1 + \frac{U_{max}}{U_S})$$

(3)

where Y_0 is the initial yielding force, U_0 the initial yielding displacement, U_H the displacement where hardening starts, U_S a parameter for controlling the degradation of the elastic stiffness of the elasto-plastic spring, U_{max} the maximum displacement experienced during the loading history, p a parameter governing the shape of the hardening branch. Fig. 2b depicts the hysteretic components F_2 when the displacement is imposed according to loading cycles of increasing amplitude.
Finally a new non-linear spring is introduced in parallel for capturing the increment of the tangential stiffness experienced by the devices at very high strain levels. This results in the F_3 contribution (Fig. 2b), defined theoretically as

$$F_3 = K_2 \left| \frac{U}{U_H} \right|^r U$$

(4)

where r is the parameter to prescribe the shape of the hardening curve, K_2 the proportional constant to describe the contribution of the hardening spring to the other springs.

3.1   Analytical approach by Lagrange equation (3-DOFS)
The reactor building is now considered as a cylindrical rigid body supported by a bed-HDRBs in an axial-symmetric configuration (see Figures 1b, 1c, 1d). The passive control system is characterized by axial and shear deformability; the state of the structure is now represented by 3 Lagrangian coordinates.

The equations of motion for the 3-DOFS arrangement can be computed by the Lagrange approach; it allows to describe the dynamic properties of any properly restrained system for small oscillations around the stable equilibrium position. The general form of the *k*-Lagrange equation can be expressed as the following [16]

$$\frac{d}{dt}\left(\frac{\partial L}{\partial \dot{q}_k}\right) - \frac{\partial L}{\partial q_k} = Q_k + Q_{D,k} \qquad (k=1,\dots,n)$$

(5)

where $L = T - V$ is the Lagrangian function, T and V are respectively the kinetic energy and the potential energy of the system, q_i are the Lagrangian coordinates, Q_k and $Q_{D,k}$ are respectively the conservative active forces and the generalized component of the damping forces.

Figure 3 depicts the system discretization where the main building of the IRIS NPP has been assumed to a cylindrical rigid body supported by the isolation system and its centroid G is generally placed into a xy reference system. At this stage the base isolation has been represented by linear springs and dashpots.
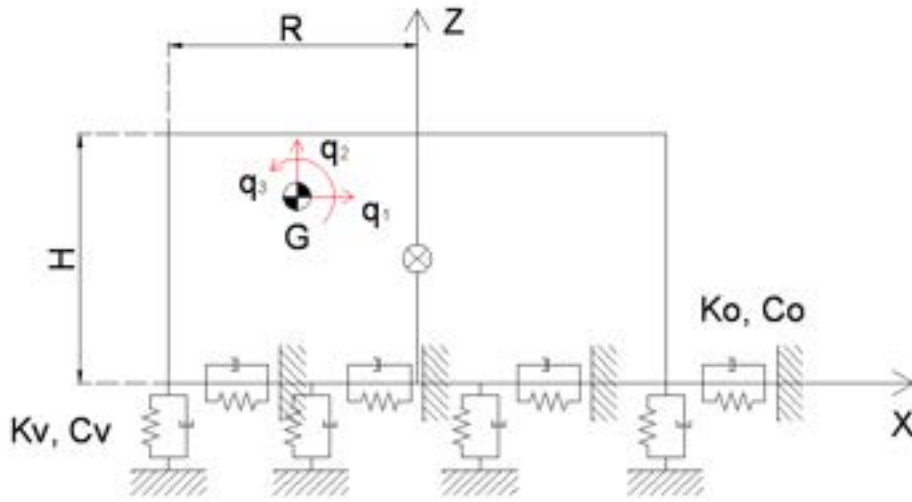

Figure 3. System discretization

The kinetic energy *T* can be expressed by the following relation (König theorem)

$$T = \frac{1}{2}m\dot{q}_1^2 + \frac{1}{2}m\dot{q}_2^2 + \frac{1}{2}I_G\dot{q}_3^2 = \frac{1}{2}\left(m\dot{q}_1^2 + m\dot{q}_2^2 + I_G\dot{q}_3^2\right)$$

(6)

it can be represented by the quadratic form [16]

$$T = \frac{1}{2}\underline{\dot{q}}^T \underline{\underline{M}}\,\underline{\dot{q}}$$

(7)

so, it is possible to define the mass matrix of the system:

$$\underline{\underline{m}} = \begin{bmatrix} m & 0 & 0 \\ 0 & m & 0 \\ 0 & 0 & I_G \end{bmatrix}$$

(8)

where m is the concentrated mass of the NPP and I_G its inertia momentum.

The potential energy expression can be obtained by effects superposition. The rigid body results supported by rheological elements and it is possible to determine the displacement components of the generic connection point P at the cylinder base. Considering different combinations for the Lagrangian coordinates, the horizontal and vertical displacements of the centroid G can be defined as follows:
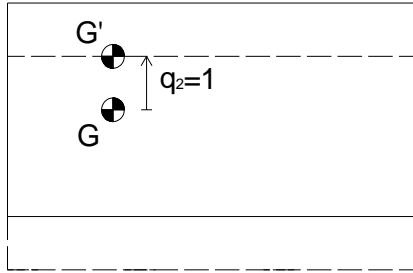
- $q_1 = 1, q_2 = q_3 = 0$
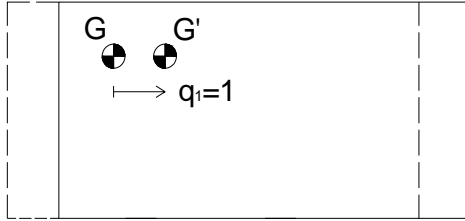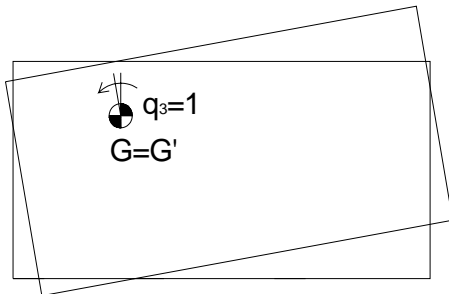

$$u_P = q_1$$
$$v_P = 0$$

- $q_2 = 1, q_1 = q_3 = 0$

$$u_P = 0$$
$$v_P = q_2$$

- $q_3 = 1, q_1 = q_2 = 0$

$$u_P = z_G q_3$$
$$v_P = (x_P - x_G) q_2$$

By effects superposition, for the generic point P under the cylinder base:
$$u_P = q_1 + z_G q_3$$
$$(9)$$

9

$$v_P = q_2 + (x_P - x_G)q_2$$
(10)

and the potential energy results

$$V = \frac{1}{2}k_o \sum_{i=1}^{n} u_i^2 + \frac{1}{2}k_v \sum_{i=1}^{n} v_i^2$$
(11)

where n represents the number of the isolators, k_o and k_v are stiffness coefficients respectively in horizontal and vertical direction. By some algebra one obtains:

$$V = \frac{1}{2}k_o \sum_{i=1}^{n}(q_1 + z_G q_3)^2 + \frac{1}{2}k_v \sum_{i=1}^{n}[q_2 + (x_i - x_G)]^2$$
(12)

$$V = \frac{1}{2}k_o \sum_{i=1}^{n}(q_1^2 + z_G^2 q_3^2 + 2z_G q_1 q_3) + \frac{1}{2}k_v \sum_{i=1}^{n}[q_2^2 + (x_i - x_G)^2 q_3^2 + 2(x_i - x_G)q_2 q_3]$$
(13)

$$V = \frac{1}{2}\left[k_o n q_1^2 + k_o n z_G^2 q_3^2 + 2k_o n z_G q_1 q_3 + k_v n q_2^2 + k_v \sum_{i=1}^{n}(x_i - x_G)^2 q_3^2 + 2k_v \sum_{i=1}^{n}(x_i - x_G)q_2 q_3\right]$$
(14)

The stiffness matrix coefficient for the 3-DOFS system are defined by the following relation [16]:

$$k_{ij} = \left[\frac{\partial^2 V}{\partial q_i \partial q_j}\right]_{q=0}$$
(15)

and they result in the stiffness matrix:

$$\underline{\underline{k}} = \begin{bmatrix} k_o n & 0 & k_o n z_G \\ 0 & k_v n & k_v \sum_{i=1}^{n}(x_i - x_G) \\ k_o n z_G & k_v \sum_{i=1}^{n}(x_i - x_G) & k_o n z_G^2 + k_v \sum_{i=1}^{n}(x_i - x_G)^2 \end{bmatrix}$$
(16)

The dissipation function is defined similarly to the potential energy definition as [16]

$$D = \frac{1}{2}c_o \sum_{i=1}^{n} \dot{u}_i^2 + \frac{1}{2}c_v \sum_{i=1}^{n} \dot{v}_i^2$$
(17)

The damping matrix coefficients are defined as

$$c_{ij} = \sum_{r=1}^{n} c_o \frac{\partial z_r}{\partial q_i} \frac{\partial z_r}{\partial q_j}$$
(18)

and they result

$$\underline{\underline{c}} = \begin{bmatrix} c_o n & 0 & c_o nz_G \\ 0 & c_v n & c_v \sum_{i=1}^{n}(x_i - x_G) \\ c_o nz_G & c_v \sum_{i=1}^{n}(x_i - x_G) & c_o nz_G + c_v \sum_{i=1}^{n}(x_i - x_G)^2 \end{bmatrix}$$

(19)

The Lagrangian component of the active forces is defined as [16]

$$\underline{Q} = -m \begin{bmatrix} a_o \\ a_v \\ 0 \end{bmatrix}$$

(20)

Finally, the system of equations of motion is expressed as following

$$\underline{\underline{m}}\ddot{\underline{q}} + \underline{\underline{c}}\dot{\underline{q}} + \underline{\underline{k}}\underline{q} = \underline{Q}$$

(21)

or, substituting eqs. 8, 16, 19, 20 in eq. 21:

$$\begin{bmatrix} m & 0 & 0 \\ 0 & m & 0 \\ 0 & 0 & I_G \end{bmatrix}\begin{bmatrix} \ddot{q}_1 \\ \ddot{q}_2 \\ \ddot{q}_3 \end{bmatrix} + \begin{bmatrix} c_o n & 0 & c_o nz_G \\ 0 & c_v n & c_v \sum_{i=1}^{n}(x_i - x_G) \\ c_o nz_G & c_v \sum_{i=1}^{n}(x_i - x_G) & c_o nz_G + c_v \sum_{i=1}^{n}(x_i - x_G)^2 \end{bmatrix}\begin{bmatrix} \dot{q}_1 \\ \dot{q}_2 \\ \dot{q}_3 \end{bmatrix} +$$

$$\begin{bmatrix} k_o n & 0 & k_o nz_G \\ 0 & k_v n & k_v \sum_{i=1}^{n}(x_i - x_G) \\ k_o nz_G & k_v \sum_{i=1}^{n}(x_i - x_G) & k_o nz_G^2 + k_v \sum_{i=1}^{n}(x_i - x_G)^2 \end{bmatrix}\begin{bmatrix} q_1 \\ q_2 \\ q_3 \end{bmatrix} = -m\begin{bmatrix} a_o \\ a_v \\ 0 \end{bmatrix}$$

And, explicitly, by the following equations:

1) $m\ddot{q}_1 + c_o n\dot{q}_1 + c_o nz_G\dot{q}_3 + k_o nq_1 + k_o nz_G q_3 = -ma_o$

(22)

2) $m\ddot{q}_2 + c_v n\dot{q}_2 + c_v \sum_{i=1}^{n}(x_i - x_G)\dot{q}_3 + k_v nq_2 + k_v \sum_{i=1}^{n}(x_i - x_G)q_3 = -ma_v$

(23)

3) $I_G\ddot{q}_3 + c_o nz_G\dot{q}_1 + c_v \sum_{i=1}^{n}(x_i - x_G)\dot{q}_2 + \left[c_o nz_G^2 + c_v \sum_{i=1}^{n}(x_i - x_G)^2\right]\dot{q}_3 + k_o nz_G q_1 + k_v \sum_{i=1}^{n}(x_i - x_G)q_2$

$$+ \left[k_o nz_G^2 + k_v \sum_{i=1}^{n}(x_i - x_G)^2\right]q_3 = 0$$

(24)

11

3.2 Implementation of the base isolation system into the 3-DOFS equations of motion

Taking now into consideration an horizontal hysteretic reaction force computed by the Abe et al. unidirectional model [11], the eq. 22, 23, 24 are rewritten by including the following replacement:

$$k_o(q_1 + z_G q_3) + c_o(\dot{q}_1 + z_G \dot{q}_3) = k_o u_P + c_o v_P = F_f$$

(25)

where F_f is the hysteretic control force relative to each passive base isolation device. In particular considering eq. 22 one obtains

$$m\ddot{q}_1 + c_o n\dot{q}_1 + c_o nz_G \dot{q}_3 + k_o nq_1 + k_o nz_G q_3 = -ma_o$$

$$m\ddot{q}_1 + n[k_o(q_1 + z_G q_3) + c_o(\dot{q}_1 + z_G \dot{q}_3)] = -ma_o$$

(26)

and the following equation results

1) $m\ddot{q}_1 + nF_f = -ma_o$

(27)

Eq. 23 involves only k_v and c_v terms and the implementation of the hysteretic elements does not change its expression.

Focusing now the attention on Eq. 24, it can be rearranged as

$$I_G \ddot{q}_3 + nz_G[k_o(q_1 + z_G q_3) + c_o(\dot{q}_1 + z_G \dot{q}_3)] + c_v \sum_{i=1}^{n}(x_i - x_G)\ddot{q}_2 + c_v \sum_{i=1}^{n}(x_i - x_G)^2 \dot{q}_3 +$$

$$k_v \sum_{i=1}^{n}(x_i - x_G)q_2 + k_v \sum_{i=1}^{n}(x_i - x_G)^2 q_3 = 0$$

(28)

where it is possible to recognize the term relative to the hysteretic control force (eq. 25). In particular F_f is now amplified by the z_G coordinate (rotational moment). The final form of Eq. 24 is

3) $I_G \ddot{q}_3 + nz_G F_f + c_v \sum_{i=1}^{n}(x_i - x_G)\dot{q}_2 + c_v \sum_{i=1}^{n}(x_i - x_G)^2 \dot{q}_3 + k_v \sum_{i=1}^{n}(x_i - x_G)q_2 + k_v \sum_{i=1}^{n}(x_i - x_G)^2 q_3 = 0$

3.3 6-DOFS generalized approach

By following the same Lagrangian approach, it is possible to write the equation of motion of the 3D IRIS base isolated NPP model including the hysteretic control forces. The Abe et al. [11] scheme allows to simulate the bidirectional response of the control device, so the equations of motion can be generalized to 6-DOFS including the whole base isolation system.

It is worth noting that in the previous 3-DOFS approach the isolation system could be assumed as a super-element under the IRIS NPP, including the characteristic of all *n*-HDRB devices, where the total reaction force was subdivided equally by *n* components. Moving to the 6-DOFS each isolator has to be considered separately and the integration of the whole equations of motion must be split into two phases

- evaluation of system state, recording displacements and velocities at the *(i)*-step for each isolators positions;
- evaluation of the control force exerted by each device for further the *(i+1)* integration step.

4.   Experiments on scaled prototypes and tuning of the model parameters

For the case of a building resting on an isolation system based on the introduction of HDRB devices, the following overall procedure is proposed, based on experimental and numerical activity, for the evaluation of the seismic fragility of the isolated IRIS NPP.

4.1   Details of the isolation system and experimental tests

Experimental tests of the behavior of the adopted HDRB devices under imposed cyclic relative displacements and constant axial force have been carried on.

Due to the very large dimensions of the HDRB elastomeric devices specifically designed for the IRIS reactor building, preliminary standard tests on ½ scaled HDRB seismic isolator prototypes (see Table 2) have been performed in two phases by the following laboratories:

- CESI-ISMES LPS (*www.cesi.it*) laboratory in Seriate (Italy);
- FIP (*www.fip-group.it*) laboratory in Selvazzano Dentro (Italy).

The first phase the experiments aimed to characterize the quasi-static and dynamic behavior of the seismic devices with constant axial loads and cyclic horizontal excitation. In this step the average shear deformation has exceeded 1.5 times the design one (100%) (see report [17] for details).

Table 2. Characteristics of the tested isolator

Isolator external diameter	500mm
Steel reinforcing plate diameter	480mm
Thickness of internal steel plates	2mm
Number of elastomeric layers	10
Thickness of an individual elastomeric layer	5mm
Total elastomeric thickness	50mm
First shape factor	24.0
Second shape factor	9.60
Full isolator height	128mm
Nominal dynamic shear modulus	1.4 MPa
Hardness	75 Shore A3
Equivalent viscous damping coefficient	10/15 %

The second phase of the experimental campaign was focused on characterizing the ultimate limit state of the seismic device (see report [18] for details). Vertical compression and shear tests up to collapse have been performed; in the latter, maximum shear deformation has exceeded 300%. Figure 4 depicts a representative outcome of a cyclic shear tests at FIP laboratory in quasi-static condition (0.005mm/s); this sample has been adopted in the remaining sections as experimental target for tuning the numerical model.
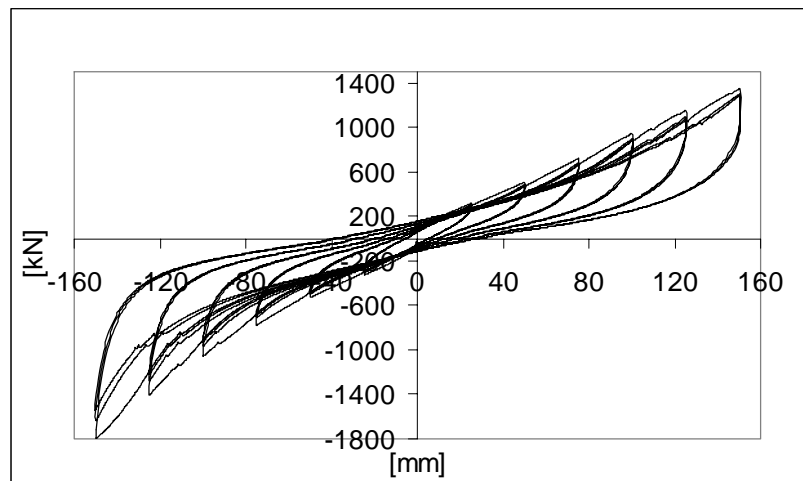

Figure 4. Cyclic shear test in quasi-static condition

4.2   *Finite element analysis*

In order to support the experimental activity and validate simplified analytical approaches, a refined finite element (FE) model was developed taking into account all significant sources of mechanical and geometrical nonlinearities. The FE model ($\approx 10^5$ DOF) allows to:

- simulate complex tests, with triaxial loading path;
- assess "first damage" conditions based on equivalent stress peaks;
- assess actual failure conditions;
- evaluate reliability and validity domain of the analytical approach developed by Corradi et al. [19] for a straightforward statement of the first damage limit state function;
- quantify the problem nonlinearity at high horizontal strain values (300%), under horizontal and vertical forces simultaneously.
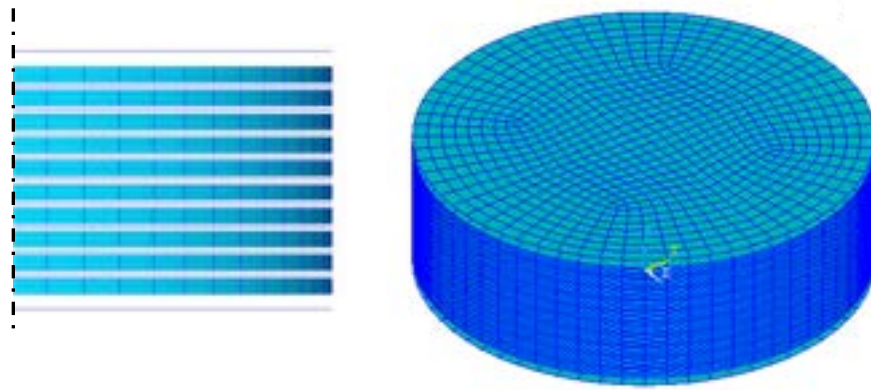

Figure 5. HDRB isolator FE model

The model, tuned against static and dynamic experimental results, has the following properties:

- *parametric geometry and mesh generation*: solid discs simulating high-damping rubber (3 elements per layer) + interposed shell elements for intermediate steel plates;
- *constraint*: shell nodes have translational DOF tied to aligned solid elements nodes by means of rigid links;
- *finite elements*: linear 3D 8-node brick element for rubber, with 3 DOF at each node, large strain capabilities, suitable for fully incompressible material; shell steel elements, with 4+4 node elements and 3+3 DOF at each node, allowing for finite membrane strains (Figure 5);
- material: 9 parameter Mooney-Rivlin nonlinear hyperelastic material.

For a more accurate evaluation of stresses, a single layer of rubber is also modeled (Figure 6):
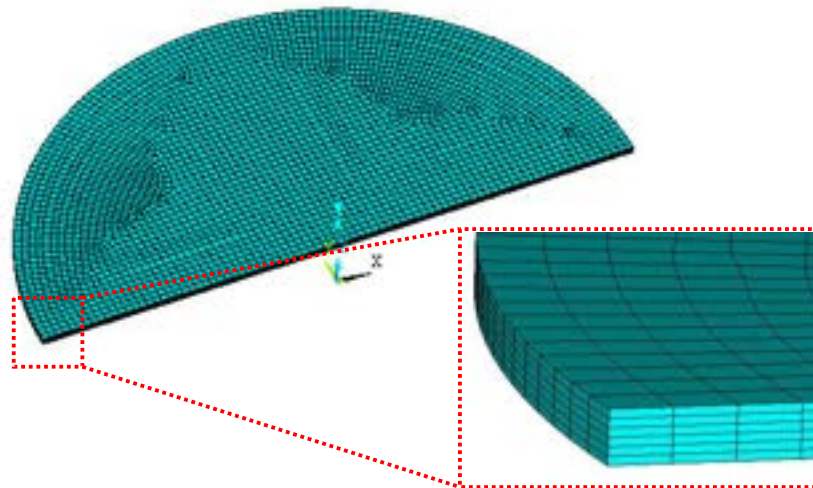

14

Figure 6. Single-layer FE model.

4.3   *Fitting of model parameters toward the numerical simulations*

The phenomenological model of the non-linear hysteretic behavior of the isolator (based on the experimental results) has been implemented to be used in the dynamic analyses for fragility estimation. Some satisfactory tests have been performed on several isolator prototypes in this respect, by adopting the model proposed by Abe et al (see also sections 2 and 3 for additional details).

For an appreciation of the model capabilities, in Figure 7a its results (thick line) are compared to the experimental behavior (thin line) of Figure 4, showing an extremely good accuracy up to an average shear deformation of about 300% (see also figure 4b and 4c where some details on 100% shear deformation cycle and 250% one are reported).
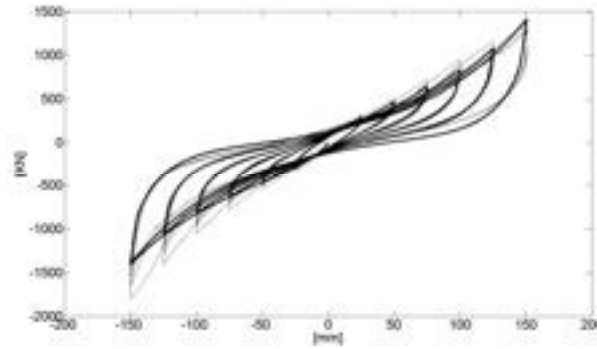
(a)
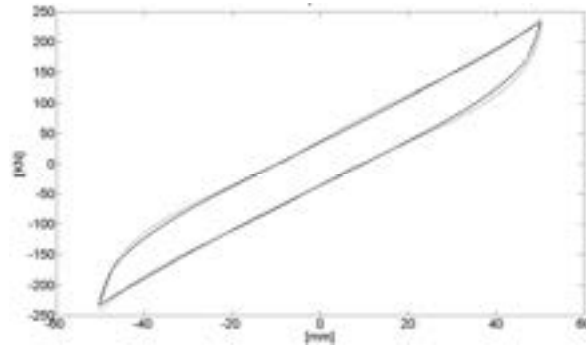
(b)
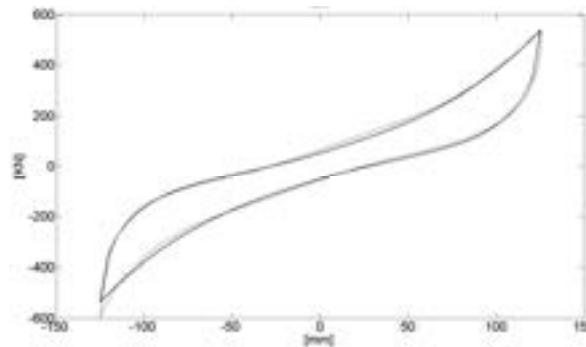
(c)

Figure 7. Isolator phenomenological model: comparison of experimental (thin line) and numerical (thick line) experimental behavior. (a) Whole cyclic experimental test (50%, 100%, 150%, 200%, 250%, 300% shear cyclic deformations and constant axial force 2000kN), (b) the second cycle detail, and the fifth one (c).

Table 3 reports the quantitative comparison between the experimental results and the numerical fitting performed by the model with reference to the cyclic loading in Figure 7a; the overall picture of the results appears satisfactory even though hysteretic damping looks slightly overestimated.

Table 3. Quantitative comparison between the experimental results and the model fitting

	Shear deformation [%]	EXPERIMENTAL		NUMERICAL	
		EQUIVALENT VISCOUS DAMPING FACTOR [%]	SECANT STIFFNESS [KN/mm]	EQUIVALENT VISCOUS DAMPING FACTOR [%]	SECANT STIFFNESS [KN/mm]
1° CYCLE	50	11.05	5.83	11.63	5.68
2° CYCLE	100	9.54	4.72	9.07	4.60
3° CYCLE	150	8.78	4.47	8.58	4.17
4° CYCLE	200	8.69	4.46	8.82	4.10
5° CYCLE	250	8.80	4.53	9.22	4.26
6° CYCLE	300	8.38	4.68	9.61	4.64

The Abe et al. [11] model parameters are finally converted from the ½ scale to the full scale for simulating the isolators into the dynamic analyses. The resulting values are the following

- $K_1 = 10000$ [KN/m]
- $\alpha = 0.1$ [m]
- $\beta = 0.3$
- $a = 4.87$ [KN]
- $b = 60$ [1/m]
- $n = 0.36$
- $Y_0 = 70$ [KN]
- $U_h = 0.06$ [m]
- $p = 2.4$
- $U_0 = 0.006$ [m]
- $U_s = 0.05$ [m]
- $K_2 = 100$ [KN/m]
- $r = 3.0$

5. Fragility analysis of isolated NPP building components

Following the PEER (Pacific Earthquake Engineering Research) approach (see [20] and included references), the annual failure rate for a mechanical component under seismic loading can be obtained from the integral:

$$P_f = \iint P\{DM > dm_f \mid EDP = edp\}\, p_{EDP}(edp \mid IM = im) p_{IM}(im) d(edp) d(im)$$

(29)

where *DM* is a Damage Measure, associated to the assumed limit state (dm_f denotes the damage level at failure), *EDP* is an Engineering Demand Parameter (support acceleration, relative displacement,…) expressing the level of the dynamic excitation imposed to the component due to the global seismic response of the structure (reactor building) and *IM* is an Intensity Measure (peak ground acceleration, spectral acceleration,…) characterizing the severity of the earthquake motion at the reactor site. As pointed out by Der Kiureghian [20] all statistics in (29) must be intended in term of annual extreme values, so that the equation delivers a risk estimate in terms of annual probability of failure of the component. For a "simple" equipment component, or for a preliminary evaluation, the limit state can be directly defined in terms of the *EDP* value at failure edp_f, thus avoiding the damage analysis step, i.e:

$$P_f = \int P\{EDP > edp_f \mid IM = im\} \, p_{IM}(im) \, d(im)$$

(30)

We shall denote in the following the fragility function $F(edp,im)$ as:

$$F(edp,im) = P\{EDP > edp \mid IM = im\} = 1 - P_{EDP}(edp/IM = im)$$

(31)

where P_{EDP} is the conditional CDF of the *edp* random variable.

When a base-isolation system based on HDRB (High Damping Rubber Bearings) is introduced (see for example Perotti et al, 2009), the acceleration values inside the building undergo a dramatic decrease. This is obtained at the price of significant relative displacements imposed to isolation devices, which are likely to become the "weakest link" in terms of seismic safety of the building; therefore the extreme value *u* of the relative displacement across the most strained isolator will be here taken as a first choice for the *edp*. The fragility function is therefore expressed as:

$$F(edp,im) = P\{U > u \mid A_g = a_g\} = P_{exc}(u, a_g)$$

(32)

The associated limit state function can be expressed in the following "capacity minus demand" format:

$$g(\mathbf{X}, u, a_g) = C - D(\mathbf{X}, a_g) = u - U(\mathbf{X}, a_g) = 0$$

(33)

where U is the random variable whose distribution delivers, for fixed random variables *X*, the result of the random vibration analysis. Note that no linearization is here exploited, since the behavior of HDRB is markedly non-linear, especially at the high level of deformations here anticipated. The random response U can be modeled through appropriate response surfaces, as functions of the basic random variables *X*. According to the well-established Response Surface Methodology (RSM [22,23]), the "true" response function is replaced by a simple analytical representation. Here, assuming that the distribution of U can be described by its mean value μ_U and its standard deviation σ_U, the so called "dual response surface" approach [24] has been adopted for modelling their dependency on *X*. Assuming that the same model can be used for the mean and the standard deviation the following response functions have been introduced:

$$\mu_U(X) = \sum_{i=1}^{m} a_i z_i(X) + \varepsilon_\mu$$

(34a)

$$\sigma_U(X) = \sum_{i=1}^{m} b_i z_i(X) + \varepsilon_\sigma$$

(34b)

where the a_i's and b_i's are coefficients to be estimated, the z_i's are usually polynomial functions and two "error" terms (ε_μ, ε_σ) are introduced as a zero mean random deviations. The latter account for the variability of estimated quantities and for the lack of fit of the adopted model, i.e. for the inadequate analytical form of the RS's and for missing variables (i.e. not comprised in (34a,b) though influencing the response). To compute the coefficients in (34a,b) a number of experiments must be run according to the chosen experimental design; at each of them the random vibration problem can be addressed via either an analytical or a simulation approach. In the second solution a sample of ground motion realizations must be generated, according to the spectral parameters appearing in *X*. For each realization, the extreme value of U is computed (e.g. via step-by-step analysis); the mean and variance of U are then estimated. The procedure is repeated for all experimental points, leading to *n* observed values for the statistical parameters of *U(X)*.

We shall assume in the following that the experiments are performed in homogeneous conditions (i.e. differing for the x_i values only), that their results are independent and that the error terms are normal with constant variance; under these hypotheses an unbiased estimate of the coefficients a_i, b_i can be obtained by the Least Square (OLS) method, independently of the variance of the ε's. An unbiased estimate of the latter terms can be subsequently obtained is defined, in terms of the residual values.

Once expressions of the type of eq. (34a,b) are established and given the properties of the basic random variable, Monte Carlo Simulations (MCS) can be applied to the evaluation of the integral delivering the exceedance probability as

$$P_{exc}(u, a_g) = \iiint_{g<0} p_U(u, \mathbf{x}) du\, d\mathbf{x}$$

(35)

Differently from the linear case, however, the RSs evaluation must be repeated for every value of peak ground acceleration, this representing, potentially, a huge computational task. It can be considered, however, that in the isolated case the seismic behavior of the building can be captured, to the aim of evaluating the isolators' behavior, by means of very simple mechanical models; the latter, in fact, can be based on the hypothesis of rigid-body motion of the building above the isolators.
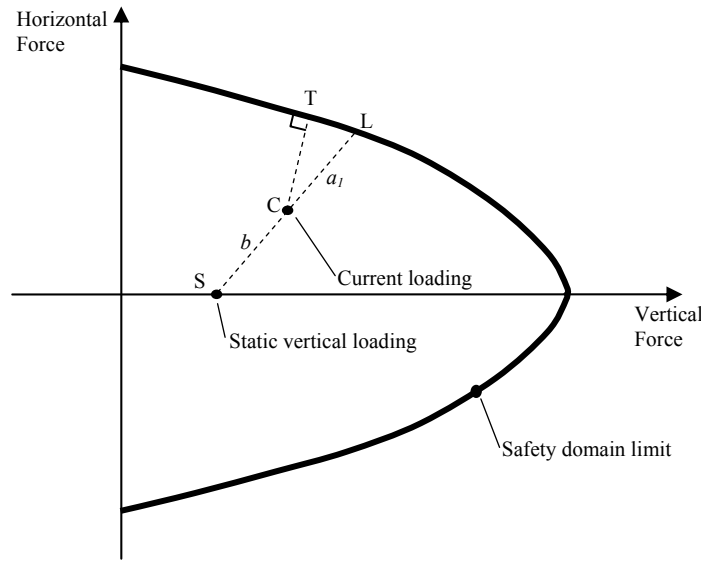

Figure 8. Limit state function for the isolator

5.1   Fragility computation via isolator limit state domain
As a second option, adopted herein, the "capacity minus demand" function - eq. (33) - can be associated to a limit state function (see [19]) expressed in terms of horizontal and vertical loads acting on the most severely strained isolator; for typical HDRBs, made by alternate rubber and steel layers, the limit state here considered is the "first damage" condition related to the attainment of an admissible peak tensile stress at the steel-rubber interface.
In this light and with reference to Figure 8, demand is here defined, at each instant, as the distance between the points describing the static vertical loading on the isolator (point S) and the current loading (point C), while capacity is computed as the total distance, measured along SC, between the static loading condition and the limit state surface (point L). Both are made non-dimensional with respect to the capacity so that the *edp* is represented by the ratio SC/SL, this being the inverse of the "instantaneous" safety factor, while the limit value *edp_f* takes a constant unit value. As an alternative, the actual distance CT can replace CL in the formulation of the safety factor.
Note that considering first damage instead of actual failure in the formulation of the limit state surface appears to be reasonable choice until a complete experimental characterization of the behavior of large HDRBs at collapse will be available.
The evaluation of the limit state domain, in terms of global vertical and horizontal forces, has been addressed in [19,25] as a delamination consequence between steel and rubber layers of the device, by accounting a tension Mohr-Coulomb approach. Such failure mechanism occurs when higher isolator shape factors (main horizontal dimensions over total rubber height) are recognized.

6.   The assumed random variables

Four independent random variables have been considered in the fragility analysis, namely
- x_1 device stiffness
- x_2 device damping
- x_3 limit domain quadratic coefficient
- x_3 limit domain constant term

6.1   Device random variables

The first two random variables (RV) account for the randomness of the dynamic properties of the isolator, represented via the model in [11]; according to this the restoring force is the sum of three contributions, i.e. an elastic-plastic model (F_2 contribution) and two elastic non-linear springs, namely a non-linear elastic spring (F_1) and an hardening spring (F_3); the model allows to reproduce analytically the experimental behavior of laminated rubber bearings. So, it results:

- RV x_1 - the stiffness of the isolator device has been varied by multiplying the stiffness parameters K_1 and a in eq. (1), K_2 in eq. (4) and dividing the initial yielding displacement U_0 in eq. (2) by the coefficients defined in the design of experiment. This random variable has lognormal distribution with 0.22 coefficient of variation (c.o.v.).
- RV x_2 - the damping of the isolator has been tuned by multiplying the initial yielding force Y_0 by the coefficients defined in the design of experiment. This random variable has lognormal distribution with 0.22 c.o.v.

A numerical sensitivity analysis has been performed by extensive cyclic simulations on the unidirectional model [11] for evaluating the variability of the original numerical stiffness and damping (Table 3 and Figure 7a) performed by the designed device prototype. Table 4 reports a brief example on the variability of the stiffness and the damping when a coefficient α has been employed in the numerical model for amplifying their intensity by using the procedure itemized above. Figure 9 depicts the hysteresis cycles resulting by the forth options considered in Table 4. It is shown how stiffness and damping into a hysteretic cycling are strictly correlated and it is impossible to vary one independently to the other one. However, the proposed procedure is able to emphasize the amplification of the selected mechanical parameter.

Table 4. Sensitivity analysis on the unidirectional model [11]

(αK_1, αK_2, U_0/α)

|	$\alpha = 1.2$		$\alpha = 1.6$	
	EQUIVALENT VISCOUS DAMPING FACTOR [%]	*SECANT STIFFNESS [KN/mm]*	*EQUIVALENT VISCOUS DAMPING FACTOR [%]*	*SECANT STIFFNESS [KN/mm]*
1° CYCLE	10.6	13.1	9	16.5
2° CYCLE	8.1	10.7	6.6	13.6
3° CYCLE	7.7	9.7	6.3	12.4
4° CYCLE	7.8	9.5	6.4	12
5° CYCLE	8.2	9.8	6.7	12.3
6° CYCLE	8.5	10.6	7	13.3

(αY_0)

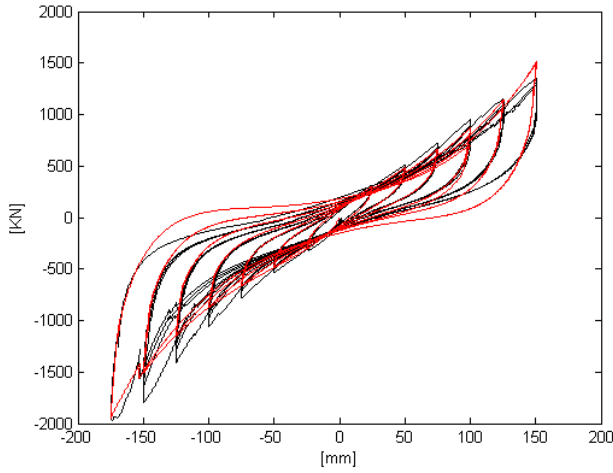|	$\alpha = 1.2$		$\alpha = 1.6$	
	EQUIVALENT VISCOUS DAMPING FACTOR [%]	*SECANT STIFFNESS [KN/mm]*	*EQUIVALENT VISCOUS DAMPING FACTOR [%]*	*SECANT STIFFNESS [KN/mm]*

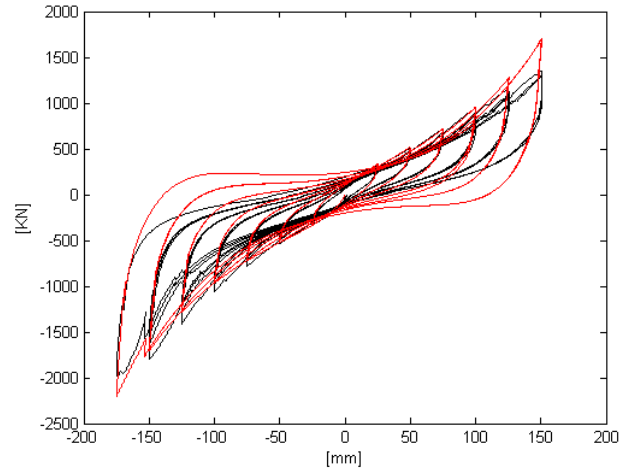|				
1° CYCLE	13.2	12	16	13.1
2° CYCLE	10.4	9.5	13	10.3
3° CYCLE	10	8.7	12.2	9.4
4° CYCLE	10	8.6	12.2	9.5
5° CYCLE	10.4	9	12.5	10.1
6° CYCLE	10.4	9.9	12.7	11.2
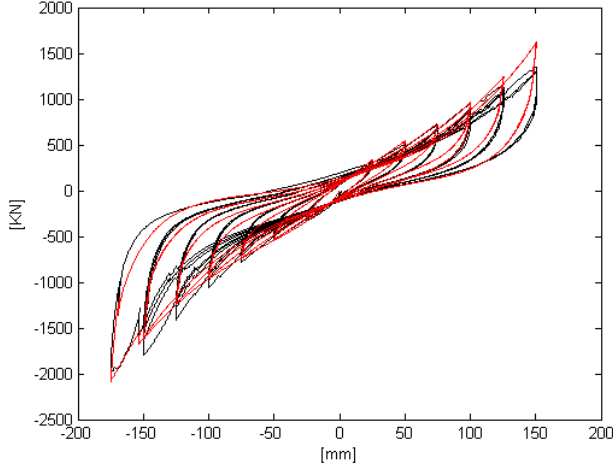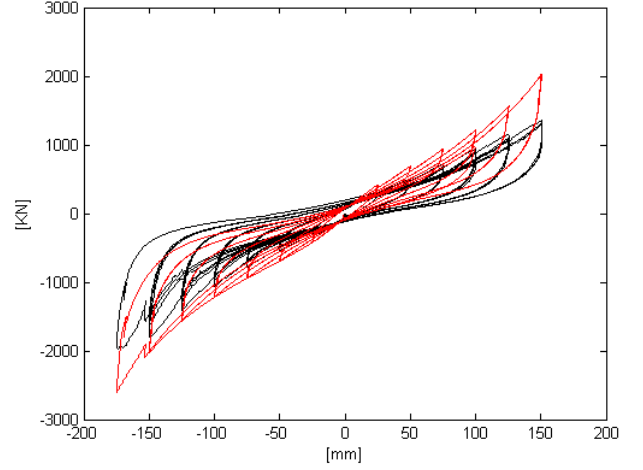
$\alpha K_1, \alpha K_2, U_0/\alpha \; ; \; \alpha = 1.2$ $\alpha K_1, \alpha K_2, U_0/\alpha \; ; \; \alpha = 1.6$

$\alpha Y_0 \; ; \; \alpha = 1.2$ $\alpha Y_0 \; ; \; \alpha = 1.6$

Figure 9. Hysteresis cycles resulting by the forth options considered in Table 4 (black line reference cycling test)

6.2   *Limit domain random variables*

The remaining two RV account for the uncertainty of the limit state function (Figure 8). A parabolic shape ($H=aV^2+c$, H horizontal reaction, V vertical reaction) has been assumed following the procedure in [19]. The coefficients of the quadratic (a) and the constant (c) terms have been taken respectively as x_3 and x_4 RVs with lognormal distribution, evaluating the reference mean value [19] and assuming the c.o.v. as 0.22. The resulting shape of the mean safety domain is depicted in Figure 10 for two reference horizontal strain levels: 300% and 400% of rubber height. The second one corresponds in particular to the first damage level evaluated in the laboratory tests and it has been adopted ($a = -0.00431$, $c = 207230.6$).
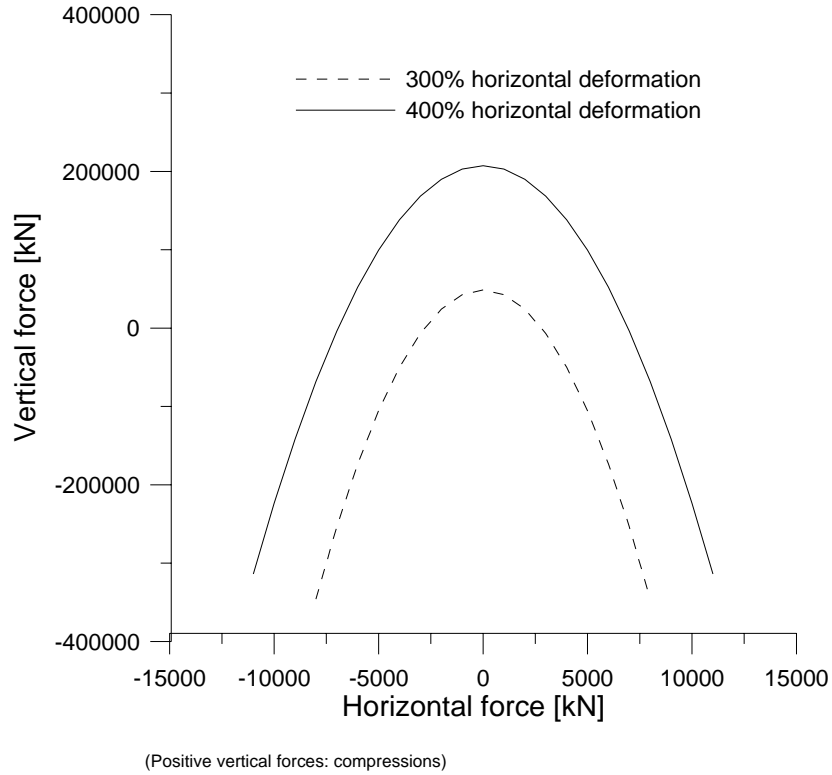
(Positive vertical forces: compressions)
Figure 10. Safety domain levels

7.   The seismic excitation

The Response Spectra prescribed by the USNRC 1.60 (1973) [26] was adopted as seismic input. The spectral parameters where treated as deterministic, so that a single set of 20 input motions, each described by three components, has been generated and used at all experimental points. Generation was performed starting from white-noise accelerograms, modulated in the time domain, and iteratively correcting their Fourier Amplitude Spectra in order to match the USNRC 1.60 (1973) curve. An example of accelerograms is given in Figure 11.
The set of 20 input motions have been prepared by this procedure for being applied to the follow probabilistic assessment on the reactor building models: in particular the 3-DOFS option implements only two components (one horizontal and one vertical), the 6-DOFS option all the seismic components (two horizontal and one vertical).
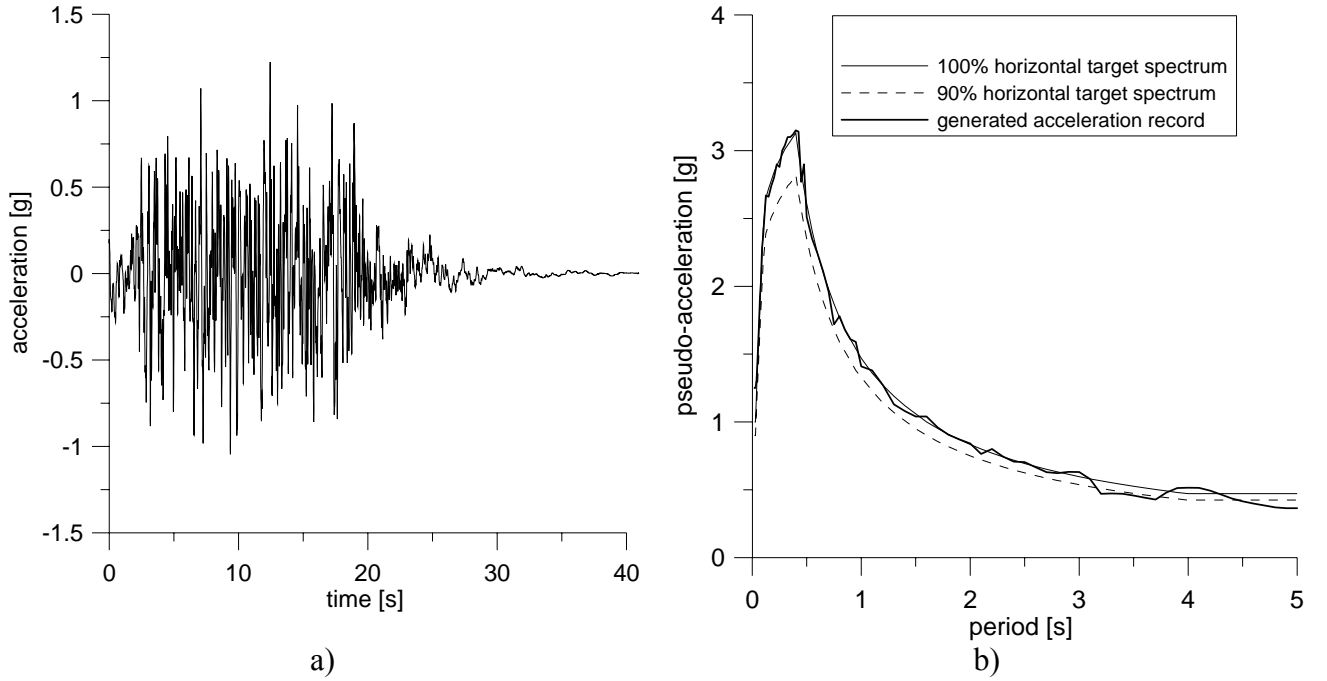
Figure 11. Example of an artificial accelerogram with the target spectra from
USNRC 1.60 (1973) – damping 5%

8.   Numerical simulations in Matlab

The 3- and 6-DOFS ordinary differential (ODE) equations of motions, accounting the isolation effects by the numerical model [11], are integrated directly by the explicit Runge-Kutta (2,3) pair of Bogacki and Shampine [27] by using the ODE23 function in Matlab. This function is useful for non stiff problems; remembering that a problem is stiff when the numerical solution has its step size limited more severely by the stability of the numerical technique than by the accuracy of the technique.

The 6-DOFS system is represented by larger computational efforts, so it has been decided to implement a greater time integration step (0.01s), with respect to the 3-DOFS system (0.005s), for limiting the time calculation of the procedure. This choice has been supported by considering the main natural frequencies of the system, efficiently captured by the selected integration step, and by testing the non linear solution accuracy.

From a quantitative point of view, if the differential system to be integrated is the following:

$$y' = f(t, y) \tag{36}$$

accounting y_n as the numerical solution at time t_n and h_n is the step size, defined by $h_n = t_{n+1} - t_n$, the one step of the Bogacki–Shampine method is given by:

$$k_1 = f(t_n, y_n)$$

$$k_2 = f(t_n + \frac{1}{2}h_n, y_n + \frac{1}{2}hk_1)$$

$$k_3 = f(t_n + \frac{3}{4}h_n, y_n + \frac{3}{4}hk_2)$$

$$y_{n+1} = y_n + \frac{2}{9}hk_1 + \frac{1}{3}hk_2 + \frac{4}{9}hk_3$$

$$k_4 = f(t_n + h_n, y_{n+1})$$

$$z_{n+1} = y_n + \frac{7}{24}hk_1 + \frac{1}{4}hk_2 + \frac{1}{3}hk_3 + \frac{1}{8}hk_4$$

(37a-f)

Here, y_{n+1} is a third-order approximation to the exact solution. On the other hand, z_{n+1} is a second-order approximation, so the difference between y_{n+1} and z_{n+1} can be also used to evaluate the suitable step size.

9.   Design of experiments: Central Composite Design

For representing the isolated building response a second-order model can be used in the application of the Response Surface Method to the structural problem [2]. A full model (i.e. encompassing all quadratic terms) requires, for k random variables, the estimation of $p=1+k+k(k+1)/2$ coefficients. In this situation the most suitable experimental strategy is the "Central Composite Design" (CCD); once fixed a "center point", CCD is the combination of a classical "two-level factorial design", in which all the combinations of two levels (high/low) of the random variables are considered, with a "Star Design". In the latter $2k$ points are considered in which one variable takes an intermediate value and the others are at the central value. Including the central point, a total number of experiments equal to $n=2^k+2k+1$ is reached. Reasoning in terms of non-dimensional zero-mean random variables $\eta_i = (x_i - \mu_{xi})/\sigma_{xi}$ while

for preserving the "rotatability" of the design the star points must be placed at $\alpha = \eta_i = \sqrt[4]{2^k} = 2$. In this study for $k=4$, it results $p=15$, $n=25$ and $\alpha = 2$.
Table 5 summarizes the design of experiments (DoE) for the selected random variables, normalized to the mean value.

Table 5. DoE with mean value normalization

Experiment	Abe et al. [11] model parameters		Safety domain	
	x_1 (stiffness)	x_2 (damping)	x_3 (a)	x_4 (c)
1	1.00	0.56	1.00	1.00
2	1.44	1.00	1.00	1.00
3	1.00	1.00	1.00	1.44
4	1.00	1.00	1.00	0.56
5	1.00	1.00	0.56	1.00
6	0.56	1.00	1.00	1.00
7	1.00	1.00	1.44	1.00
8	1.00	1.44	1.00	1.00
9	1.61	0.59	0.59	1.61
10	1.61	0.59	0.59	0.59
11	0.59	0.59	0.59	1.61
12	0.59	0.59	0.59	0.59
13	0.59	0.59	1.61	0.59

14	1.61	0.59	1.61	1.61
15	0.59	0.59	1.61	1.61
16	1.61	0.59	1.61	0.59
17	1.61	1.61	0.59	1.61
18	1.61	1.61	0.59	0.59
19	0.59	1.61	0.59	1.61
20	0.59	1.61	0.59	0.59
21	0.59	1.61	1.61	0.59
22	1.61	1.61	1.61	1.61
23	0.59	1.61	1.61	1.61
24	1.61	1.61	1.61	0.59
25	1.00	1.00	1.00	1.00

10. Application of the response surface method

Running the experiments detailed in Table 4, spanning from lower (0.3g) to higher (1.1g) values of seismic peak ground acceleration, it is possible to compute the extreme structural response in terms of mean and standard deviation of the ratio SC/SL (see Figure 8). In particular the most strained device in the whole isolation system has been selected step by step for each PGA. Tables 6 and 7 report the 25 experiments for the central composite design with the resulting mean and standard deviation, respectively for the 3-DOFS and 6-DOFS model option: the last one presents always higher mean and standard deviation levels due to the input characteristic: the horizontal resultant is generally more intense.

Table 6. 3-DOFS: mean and standard deviation of the ratio SC/SL for each PGA level

PGA [g]	0.3		0.4		0.5	
Experiment	E (SC/SL)	σ (SC/SL)	E (SC/SL)	σ (SC/SL)	E (SC/SL)	σ (SC/SL)
1	0.3548	0.0557	0.5624	0.1190	0.8485	0.1597
2	0.3346	0.0383	0.5068	0.0635	0.7171	0.1117
3	0.2365	0.0424	0.3663	0.0768	0.5273	0.1060
4	0.3910	0.0717	0.6040	0.1280	0.8650	0.1771
5	0.2160	0.0396	0.3337	0.0707	0.4780	0.0978
6	0.2406	0.0406	0.3750	0.0528	0.5471	0.1045
7	0.3424	0.0613	0.5301	0.1112	0.7632	0.1535
8	0.2646	0.0444	0.3994	0.0783	0.5542	0.1094
9	0.2678	0.0293	0.4071	0.0553	0.6111	0.1281
10	0.4576	0.0504	0.6948	0.0966	1.0553	0.2260
11	0.1697	0.0339	0.2681	0.0538	0.3905	0.0869
12	0.2865	0.0602	0.4547	0.0985	0.6657	0.1544
13	0.4713	0.0944	0.7449	0.1498	1.0851	0.2416
14	0.4394	0.0488	0.6702	0.0909	0.9971	0.2082
15	0.2806	0.0545	0.4416	0.0857	0.6422	0.1387
16	0.7441	0.0812	1.1312	0.1538	1.6986	0.3563
17	0.1731	0.0211	0.2613	0.0402	0.3620	0.0583
18	0.2948	0.0377	0.4451	0.0725	0.6191	0.1013
19	0.1366	0.0224	0.2098	0.0422	0.2938	0.0651
20	0.2301	0.0375	0.3587	0.0735	0.5027	0.1113
21	0.3794	0.0623	0.5830	0.1174	0.8165	0.1810
22	0.2855	0.0343	0.4307	0.0644	0.5959	0.0948
23	0.2259	0.0383	0.3443	0.0693	0.4822	0.1069
24	0.4809	0.0586	0.7259	0.1120	1.0061	0.1620
25	0.2862	0.0516	0.4429	0.0932	0.6368	0.1286

PGA [g]	0.6		0.7		0.8	
Experiment	E (SC/SL)	σ (SC/SL)	E (SC/SL)	σ (SC/SL)	E (SC/SL)	σ (SC/SL)
1	1.1204	0.2652	1.4273	0.2813	1.6693	0.4312
2	0.9312	0.1616	1.1623	0.2217	1.4642	0.3081
3	0.7030	0.1341	0.8966	0.1702	1.0925	0.2013
4	1.1535	0.2192	1.4794	0.2817	1.8142	0.3450
5	0.6374	0.1211	0.8173	0.1556	1.0021	0.1903
6	0.7140	0.1482	0.9277	0.1793	1.1462	0.2139
7	1.0175	0.1941	1.2977	0.2463	1.5813	0.2914
8	0.7388	0.1320	0.9465	0.1790	1.1668	0.2020
9	0.7732	0.1852	1.0398	0.3189	1.3705	0.3470
10	1.3308	0.3330	1.7718	0.5723	2.3545	0.6149
11	0.5427	0.1567	0.6756	0.1579	0.8711	0.1995
12	0.9225	0.2766	1.1545	0.2726	1.4879	0.3583
13	1.5079	0.4358	1.8772	0.4390	2.4204	0.5551
14	1.2639	0.2980	1.7101	0.5066	2.2433	0.5600
15	0.8920	0.2531	1.1116	0.2560	1.4330	0.3194
16	2.1490	0.5152	2.8891	0.8875	3.8092	0.9651
17	0.4772	0.0731	0.6091	0.0935	0.7567	0.1318
18	0.8150	0.1306	1.0513	0.1655	1.3064	0.2355
19	0.3804	0.0837	0.5023	0.0964	0.6239	0.1119
20	0.6462	0.1452	0.8561	0.1683	1.0635	0.1937
21	1.0569	0.2328	1.3958	0.2679	1.7337	0.3111
22	0.7818	0.1195	0.9950	0.1504	1.2333	0.2107
23	0.6261	0.1371	0.8242	0.1580	1.0256	0.1843
24	1.3261	0.2033	1.6930	0.2601	2.1033	0.3668
25	0.8489	0.1614	1.0843	0.2059	1.3241	0.2463

PGA [g]	0.9		1		1.1	
Experiment	E (SC/SL)	σ (SC/SL)	E (SC/SL)	σ (SC/SL)	E (SC/SL)	σ (SC/SL)
1	2.1410	0.6236	2.6760	0.5628	3.1225	0.7929
2	1.7690	0.3760	2.1489	0.4387	2.4379	0.5397
3	1.2510	0.1997	1.5016	0.2679	1.8105	0.3308
4	2.0788	0.3484	2.4836	0.4697	2.9983	0.5863
5	1.1482	0.1921	1.3720	0.2589	1.6562	0.3233
6	1.4095	0.2561	1.6832	0.2936	1.9133	0.3214
7	1.8107	0.2892	2.1733	0.3879	2.6205	0.4791
8	1.3855	0.2109	1.6390	0.2186	1.9139	0.3262
9	1.6360	0.2851	2.2373	0.7759	2.7612	0.9252
10	2.8195	0.5185	3.8364	1.3432	4.7705	1.6649
11	1.1193	0.2723	1.2761	0.2859	1.4919	0.4177
12	1.9278	0.5003	2.1908	0.5173	2.5840	0.7519
13	3.1109	0.7586	3.5468	0.7955	4.1474	1.1627
14	2.6826	0.4521	3.6676	1.2635	4.4988	1.4656
15	1.8320	0.4237	2.0884	0.4519	2.4296	0.6608
16	4.5467	0.7940	6.2179	2.1568	7.6756	2.5749
17	0.9166	0.1582	1.0930	0.1798	1.2892	0.2159
18	1.5776	0.2864	1.8841	0.3279	2.2215	0.3897
19	0.7160	0.1520	0.8284	0.1728	0.9750	0.1896
20	1.2184	0.2521	1.4100	0.2849	1.6525	0.3120
21	1.9895	0.4218	2.3017	0.4796	2.7089	0.5261
22	1.5000	0.2520	1.7907	0.2812	2.1070	0.3433
23	1.1774	0.2558	1.3654	0.2881	1.6045	0.3228
24	2.5476	0.4401	3.0379	0.5008	3.5831	0.6010
25	1.5172	0.2457	1.8184	0.3301	2.1918	0.4111

Table 7. 6-DOFS: mean and standard deviation of the ratio SC/SL for each PGA level

PGA [g]	0.3		0.4		0.5	
Experiment	E (SC/SL)	σ (SC/SL)	E (SC/SL)	σ (SC/SL)	E (SC/SL)	σ (SC/SL)
1	0.4158	0.0484	0.6775	0.0899	0.9907	0.1200
2	0.3939	0.0301	0.5908	0.0488	0.8347	0.0821
3	0.2833	0.0305	0.4387	0.0549	0.6231	0.0837
4	0.4763	0.0514	0.7375	0.0921	1.0472	0.1402
5	0.2630	0.0284	0.4072	0.0508	0.5782	0.0774
6	0.2999	0.0484	0.4447	0.0741	0.6477	0.1257
7	0.4101	0.0442	0.6351	0.0795	0.9020	0.1212
8	0.3164	0.0347	0.4766	0.0624	0.6655	0.0973
9	0.3094	0.0328	0.5075	0.0707	0.7778	0.1379
10	0.5401	0.0574	0.8856	0.1237	1.3566	0.2401
11	0.2075	0.0339	0.3350	0.0590	0.4877	0.0942
12	0.3624	0.0588	0.5852	0.1034	0.8516	0.1645
13	0.5771	0.0943	0.9316	0.1642	1.3562	0.2618
14	0.5003	0.0530	0.8207	0.1141	1.2580	0.2231
15	0.3356	0.0551	0.5415	0.0952	0.7884	0.1521
16	0.8604	0.0913	1.4113	0.1966	2.1627	0.3833
17	0.2120	0.0229	0.3194	0.0391	0.4460	0.0565
18	0.3699	0.0400	0.5570	0.0677	0.7778	0.0978
19	0.1662	0.0316	0.2540	0.0412	0.3541	0.0559
20	0.2905	0.0555	0.4446	0.0711	0.6192	0.0974
21	0.4621	0.0878	0.7065	0.1146	0.9846	0.1554
22	0.3430	0.0372	0.5167	0.0634	0.7216	0.0918
23	0.2686	0.0509	0.4104	0.0671	0.5718	0.0905
24	0.5895	0.0638	0.8882	0.1086	1.2403	0.1570
25	0.3449	0.0372	0.5341	0.0668	0.7586	0.1018

PGA [g]	0.7		0.8		0.9	
Experiment	E (SC/SL)	σ (SC/SL)	E (SC/SL)	σ (SC/SL)	E (SC/SL)	σ (SC/SL)
1	1.6405	0.2582	2.1153	0.4335	2.8542	0.7393
2	1.3859	0.1865	1.7293	0.1939	2.1599	0.3672
3	1.0446	0.1511	1.2861	0.1690	1.5163	0.1800
4	1.7542	0.2530	2.1596	0.2822	2.5464	0.3020
5	0.9686	0.1397	1.1925	0.1558	1.4060	0.1668
6	1.1238	0.2233	1.3504	0.2474	1.6245	0.2756
7	1.5122	0.2188	1.8618	0.2446	2.1949	0.2606
8	1.1611	0.1672	1.4261	0.2036	1.7210	0.2301
9	1.5032	0.3618	1.8630	0.6014	2.5985	0.7681
10	2.6238	0.6335	3.2538	1.0535	4.5404	1.3419
11	0.8443	0.1501	1.0978	0.1602	1.3229	0.2159
12	1.4725	0.2636	1.9169	0.2787	2.3108	0.3754
13	2.3475	0.4174	3.0526	0.4453	3.6785	0.6003
14	2.4300	0.5839	3.0108	0.9701	4.1983	1.2412
15	1.3656	0.2417	1.7744	0.2594	2.1377	0.3498
16	4.1798	1.0062	5.1804	1.6725	7.2258	2.1359
17	0.7386	0.0989	0.9209	0.1335	1.1299	0.1571
18	1.2886	0.1707	1.6067	0.2336	1.9724	0.2741
19	0.6169	0.1087	0.7672	0.1251	0.8975	0.1496
20	1.0771	0.1898	1.3395	0.2167	1.5663	0.2609
21	1.7155	0.3022	2.1332	0.3479	2.4956	0.4160
22	1.1943	0.1609	1.4894	0.2154	1.8265	0.2539
23	0.9975	0.1757	1.2400	0.2033	1.4511	0.2420
24	2.0537	0.2748	2.5607	0.3712	3.1417	0.4368
25	1.2714	0.1838	1.5653	0.2053	1.8454	0.2190

PGA [g]	1.1	
Experiment	E (SC/SL)	σ (SC/SL)
1	4.2553	0.9807
2	3.2456	0.5047
3	2.2643	0.3569
4	3.8062	0.6000
5	2.1016	0.3313
6	2.3182	0.4739
7	3.2778	0.5166
8	2.3911	0.3263
9	3.9414	1.6361
10	6.8933	2.8667
11	1.8406	0.3962
12	3.2143	0.6925
13	5.1181	1.1017
14	6.3645	2.6390
15	2.9748	0.6399
16	10.9603	4.5499
17	1.6397	0.1940
18	2.8630	0.3390
19	1.2521	0.2472
20	2.1854	0.4315
21	3.4818	0.6875
22	2.6502	0.3136
23	2.0243	0.3997
24	4.5594	0.5395
25	2.7567	0.4345

A specific RS must be computed for each considered PGA and it is a distinctive procedure of the non linear configuration. On the contrary, for the linear approach, typically applied to non isolated reactor buildings, it is sufficient evaluating one RS for a certain PGA level and deriving the other RSs by interpolation.

The so called "dual response surface" approach for solving the reliability problem under stochastic input is herein adopted. The analytical expression of the generic response surface has the following form for both the mean and the standard deviation surface:

$$g(\underline{x}) = a_0 + a_1 x_1 + a_2 x_2 + a_3 x_3 + a_4 x_4 + a_5 x_1 x_2 + a_6 x_1 x_3 + a_7 x_1 x_4 + a_8 x_2 x_3 + a_9 x_2 x_4 + a_{10} x_3 x_4 +$$
$$+ a_{11} x_1^2 + + a_{12} x_2^2 + a_{13} x_3^2 + a_{14} x_4^2$$

(38)

In other words, the mean and the standard deviation value of the maximum ratio SC/SL (this last recorded in the most strained device of whole isolation system during each realization) over 20 time histories is evaluated for each design point. In light of these considerations several RSs, function of four random variables and the input PGA, have been processed by an ordinary least squares (OLS) method.

Tables 8 and 9 reports the RS coefficient calculated by OLS method for the 3-DOFS configuration, in the range of considered PGA, respectively for the mean and the standard deviation values. By the same, Tables 10 and 11 for the 6-DOFS structural model. This set of RSs allows to define a series of *meta-models* useful in the remaining of this report for performing fragility analyses on the isolated reactor building.

Table 8. 3-DOFS: mean RS coefficients for each PGA level

PGA [g]	0.3	0.4	0.5	0.6	0.7	0.8	0.9	1.0	1.1
a_0	0.28032	0.47724	0.72932	1.09656	1.32180	1.92557	3.02343	3.19535	3.76347

a_1	0.22709	0.35670	0.54195	0.76059	0.99912	0.81540	0.24414	0.59017	1.45682
a_2	-0.18526	-0.35582	-0.64749	-0.96345	-1.06827	-0.91987	-2.44640	-2.84500	-2.93103
a_3	0.30590	0.48484	0.73519	0.93933	1.15024	1.14386	1.70307	2.10916	1.95177
a_4	-0.32813	-0.51581	-0.71650	-1.05396	-1.37089	-1.94875	-1.86445	-1.97857	-2.97467
a_5	0.00526	-0.01170	0.00036	-0.09570	-0.05600	0.20055	0.45075	0.80154	0.76475
a_6	-0.10517	-0.14974	-0.25913	-0.22878	-0.43208	-0.62704	-0.54405	-1.18576	-1.62165
a_7	0.05510	0.08110	0.11942	0.13324	0.20092	0.26014	0.30193	0.52355	0.66981
a_8	-0.06130	-0.08330	-0.13042	-0.15020	-0.20652	-0.28897	-0.32380	-0.54132	-0.70425
a_9	0.08420	0.15356	0.27650	0.36002	0.45894	0.38993	0.92616	1.24403	1.32124
a_{10}	-0.05160	-0.08400	-0.13672	-0.18370	-0.25165	-0.35691	-0.45346	-0.64959	-0.79319
a_{11}	0.05650	0.08880	0.15631	0.20500	0.25959	0.37128	0.49444	0.69547	0.88975
a_{12}	-0.03160	-0.05220	-0.08670	-0.08580	-0.08800	0.05150	-0.07180	-0.11750	0.10702
a_{13}	-0.07680	-0.11702	-0.16785	-0.22344	-0.28820	-0.36947	-0.44072	-0.54966	-0.66298
a_{14}	0.11407	0.17338	0.22623	0.34075	0.45139	0.65909	0.53339	0.54268	0.92265

Table 9. 3-DOFS: standard deviation RS coefficients for each PGA level

PGA [g]	0.3	0.4	0.5	0.6	0.7	0.8	0.9	1.0	1.1
a_0	0.07540	0.10699	0.21899	0.57440	0.44030	0.62863	1.11669	1.04662	1.68766
a_1	0.08490	0.30835	0.18591	0.07250	0.15156	0.18983	-0.00313	0.04000	0.32844
a_2	-0.02580	-0.16409	-0.10060	-0.51858	-0.14401	-0.70216	-1.94466	-0.38383	-1.40198
a_3	0.03200	0.04990	0.06160	0.13586	0.08270	0.28731	0.65404	-0.03610	0.04960
a_4	-0.11829	-0.20141	-0.27412	-0.32097	-0.42995	-0.34309	-0.03270	-0.79562	-1.01646
a_5	-0.04430	-0.13991	-0.03080	0.01260	0.14397	0.09410	0.02880	0.59004	0.50572
a_6	0.00590	-0.00448	-0.08250	-0.06890	-0.28491	-0.21893	-0.01030	-0.82210	-0.83084
a_7	-0.00254	0.00084	0.01510	0.00503	0.05880	0.06740	0.00115	0.20864	0.20062
a_8	0.00281	0.00144	-0.01510	-0.01230	-0.07970	-0.07910	-0.01970	-0.22530	-0.26821
a_9	0.00021	0.06400	0.04690	0.19033	0.08970	0.29623	0.75443	0.29418	0.64303
a_{10}	-0.00751	-0.00982	-0.03450	-0.07060	-0.11264	-0.11503	-0.07300	-0.28235	-0.34783
a_{11}	0.00937	0.01320	0.04330	0.08590	0.13054	0.14119	0.13588	0.31610	0.44555
a_{12}	0.00557	0.00832	0.02940	0.03900	0.08180	-0.00042	-0.14927	0.25023	0.28656
a_{13}	-0.01000	-0.01780	-0.03350	-0.04700	-0.06640	-0.07430	-0.07940	-0.14277	-0.17044
a_{14}	0.04160	0.07250	0.09190	0.08040	0.13334	0.07800	-0.09850	0.24256	0.27428

Table 10. 6-DOFS: mean RS coefficients for each PGA level

PGA [g]	0.3	0.4	0.5	0.7	0.8	0.9	1.1
a_0	0.40947	0.73645	1.12704	2.05909	2.93084	3.66000	4.61979
a_1	0.19526	0.44836	0.56827	0.74296	1.00838	1.28657	2.66833
a_2	-0.19438	-0.48932	-0.73945	-0.95929	-1.89482	-3.59547	-4.59323
a_3	0.34331	0.48230	0.68554	0.94996	1.17029	1.75463	2.54247
a_4	-0.44047	-0.75502	-1.08094	-1.97164	-2.46494	-2.33104	-3.51244
a_5	0.01982	-0.01612	0.06228	0.42957	0.43303	0.90390	1.23460
a_6	-0.09580	-0.18293	-0.33754	-0.92048	-1.05011	-1.78545	-2.92272
a_7	0.06078	0.09883	0.16005	0.32740	0.38428	0.63256	1.03795
a_8	-0.06693	-0.10719	-0.17114	-0.35081	-0.41606	-0.67992	-1.12151
a_9	0.07752	0.20052	0.31022	0.49525	0.86877	1.75044	2.34515
a_{10}	-0.05465	-0.10640	-0.18485	-0.39991	-0.51077	-0.75559	-1.14532
a_{11}	0.06283	0.12134	0.20906	0.43861	0.56452	0.84350	1.29846
a_{12}	-0.03330	-0.01614	-0.00856	0.12587	0.18509	0.09462	0.10923
a_{13}	-0.08922	-0.14168	-0.20703	-0.37282	-0.46793	-0.59585	-0.86793
a_{14}	0.15205	0.25744	0.35832	0.65126	0.79420	0.65423	1.03373

Table 11. 6-DOFS: standard deviation RS coefficients for each PGA level

PGA [g]	0.3	0.4	0.5	0.7	0.8	0.9	1.1
a_0	0.12990	0.22297	0.35710	0.51338	0.59202	0.82298	1.53995
a_1	-0.05222	-0.02672	-0.16411	-0.20207	0.04326	0.08824	0.18166
a_2	-0.06211	-0.12990	-0.04847	-0.03600	-0.59002	-1.85794	-0.87744
a_3	0.02709	0.03429	0.02706	0.05648	0.10713	0.58251	-0.13196
a_4	-0.06580	-0.13606	-0.23353	-0.35015	-0.21576	0.26484	-0.93255

a_5	0.02540	0.02560	0.12540	0.35450	0.51323	0.63801	1.47036
a_6	-0.01276	-0.02321	-0.07414	-0.37919	-0.73557	-0.92778	-2.20988
a_7	-0.00337	0.00505	0.02086	0.08838	0.19313	0.23898	0.50552
a_8	0.00441	-0.00381	-0.01854	-0.08824	-0.19851	-0.24977	-0.52892
a_9	0.02960	0.05018	0.01313	0.08391	0.43247	1.02551	0.86188
a_{10}	-0.00483	-0.01927	-0.04914	-0.12202	-0.20121	-0.26682	-0.63950
a_{11}	0.00515	0.02233	0.05170	0.13475	0.22250	0.30306	0.70352
a_{12}	0.00877	0.02124	0.05065	0.09181	0.09652	-0.07591	0.47003
a_{13}	-0.01217	-0.02140	-0.03525	-0.07290	-0.10274	-0.12725	-0.25102
a_{14}	0.01863	0.04157	0.07190	0.09839	0.03284	-0.21660	0.21101

11. Fragility analysis

The fragility functions have been computed by the "hit or miss" Monte Carlo Method (MCM) [2,28]. The RSs support the computational procedures. In particular the application of the MCM consists in a sequential generation of samples of lognormal variables (x_1 x_2 x_3 x_4).

Taking into account the probabilistic parameters of a lognormal distributed random variable, one can evaluate the parameters of the variable's natural logarithm (by definition, the variable's logarithm is normally distributed) as

$$\bar{a} = \ln(M(x) + 0.5\ln\left(1 + \frac{\Sigma(x)}{M(x)^2}\right) \tag{39}$$

$$\sigma^2 = \ln\left(1 + \frac{\Sigma(x)}{M(x)^2}\right) \tag{40}$$

where $\bar{a}$ and σ are the mean and standard deviation of the variable's natural logarithm. Table 12 reports the main normalized random variables statistic parameters where x is a generic random variable with a lognormal distribution, then $y = \ln(x)$ has a normal distribution.

Table 12. Normalized random variables statistic parameters

	Lognormal	Normal
x_1	$M(x)=1$ $\Sigma(x)=0.22$	$\bar{a}=-0.02363$ $\sigma=0.217406$ $\Sigma^2=0.047265$
x_2	$M(x)=1$ $\Sigma(x)=0.22$	$\bar{a}=-0.02363$ $\sigma=0.217406$ $\Sigma^2=0.047265$
x_3	$M(x)=1$ $\Sigma(x)=0.22$	$\bar{a}=-0.02363$ $\sigma=0.217406$ $\Sigma^2=0.047265$
x_4	$M(x)=1$ $\Sigma(x)=0.22$	$\bar{a}=-0.02363$ $\sigma=0.217406$ $\Sigma^2=0.047265$

For each sample extracted by the lognormal distributions it is possible to evaluate, by the mean and standard deviation response surfaces, the probability density function of the maximum ratio SC/SL (Figure 8). The mean and standard deviation computed via the RSs are subsequently used for extracting the extreme value from the Gumbel distribution. The extracted value is finally compared to the critical threshold. By this procedure the exceedance probability is evaluated and the MCM fragility curve is completed.

Figure 12 depicts the fragility functions processed by MCM for the 3-DOFS structural model. The fragility is represented as the probability of exceeding the limit state domain. Figure 13 presents a comparison between the fragility curves respectively for 3- and 6-DOFS.
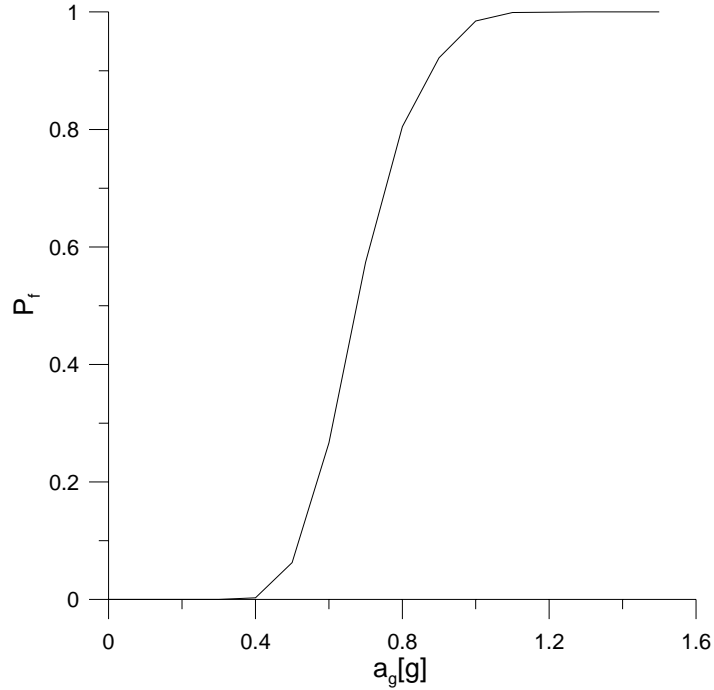

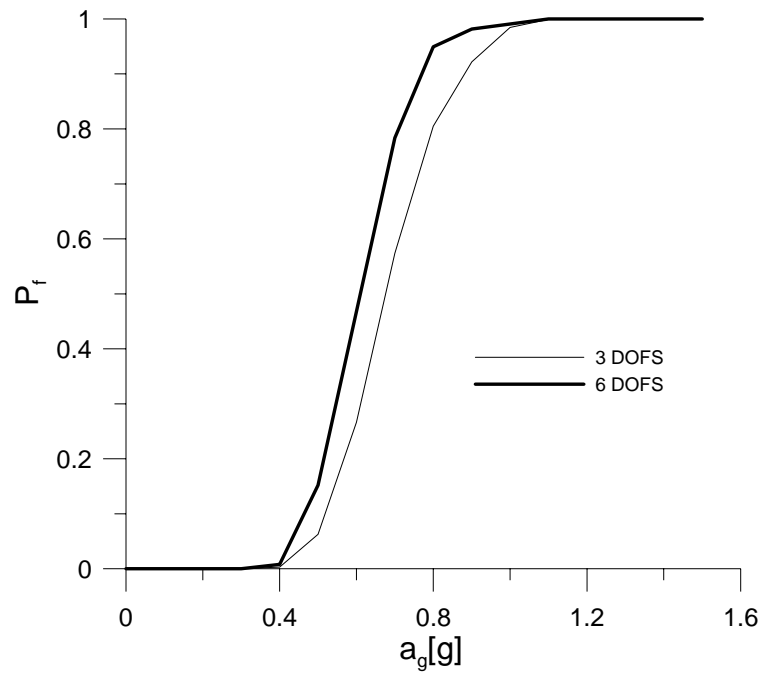Figure 12. MCM fragility function for the 3-DOFS model

Figure 13. Comparison: MCM fragility functions for the 3- and 6-DOFS models

The 6-DOFS system emphasizes more fragility than the 3-DOFS due to the different weight of the seismic input. The 3-DOFS presents only one component in the horizontal direction;

instead, the 6-DOFS implements the resultant of both horizontal components. This last horizontal resulting force is in general more intense than the single component; even if, formally, both the inputs are characterized by the same PGA.

12.   Application to the computation of seismic risk

The remaining of this report is devoted to the evaluation of the seismic risk by integrating the hazard and fragility evaluations. In particular both the fragility function of the maximum ratio SC/SL for 3- and 6-DOFS models are considered.

The problem of establishing the hazard curve is complex due to the fact the statistical parameters over a certain limit, in terms of return period, lacks of observable data. Therefore, some assumptions have been introduced. The hazard is related to a site described by return period vs ground acceleration in Figure 14.

In the estimation of the seismic risk two hypotheses has been introduced:

1) the PDF (probability density function, Figure 15) for the hazard is extended and truncated to 16m/s^2 (Figure 16);

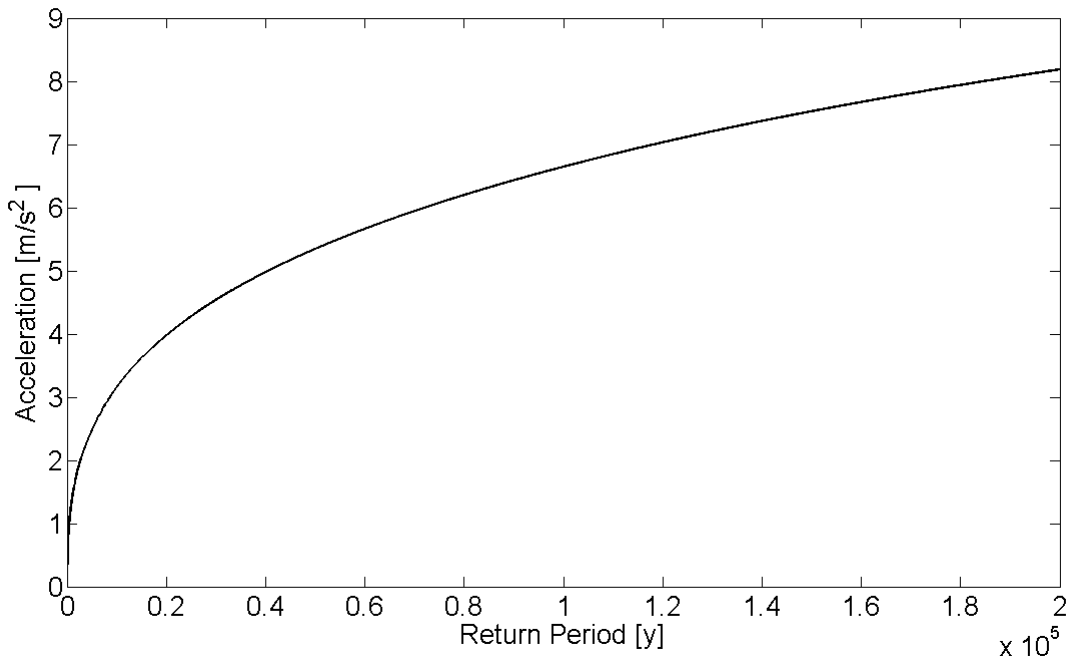2) the PDF is extended to 20m/s^2 and it is not truncated (Figure 17).
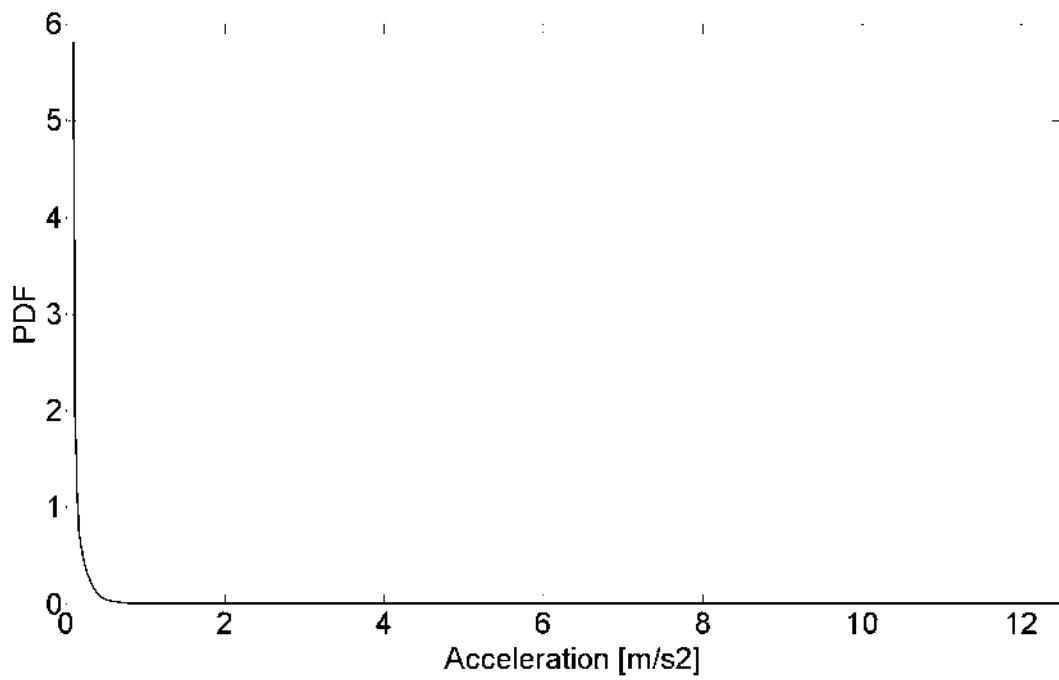

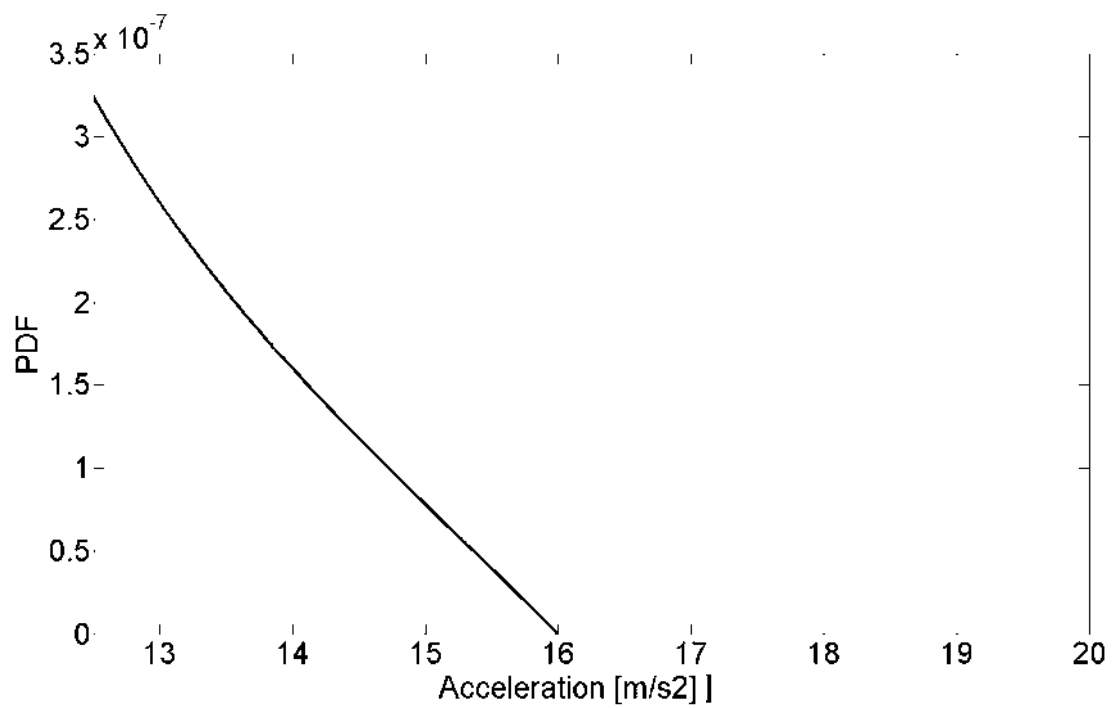Figure 14. Seismic hazard

Figure 15. PDF

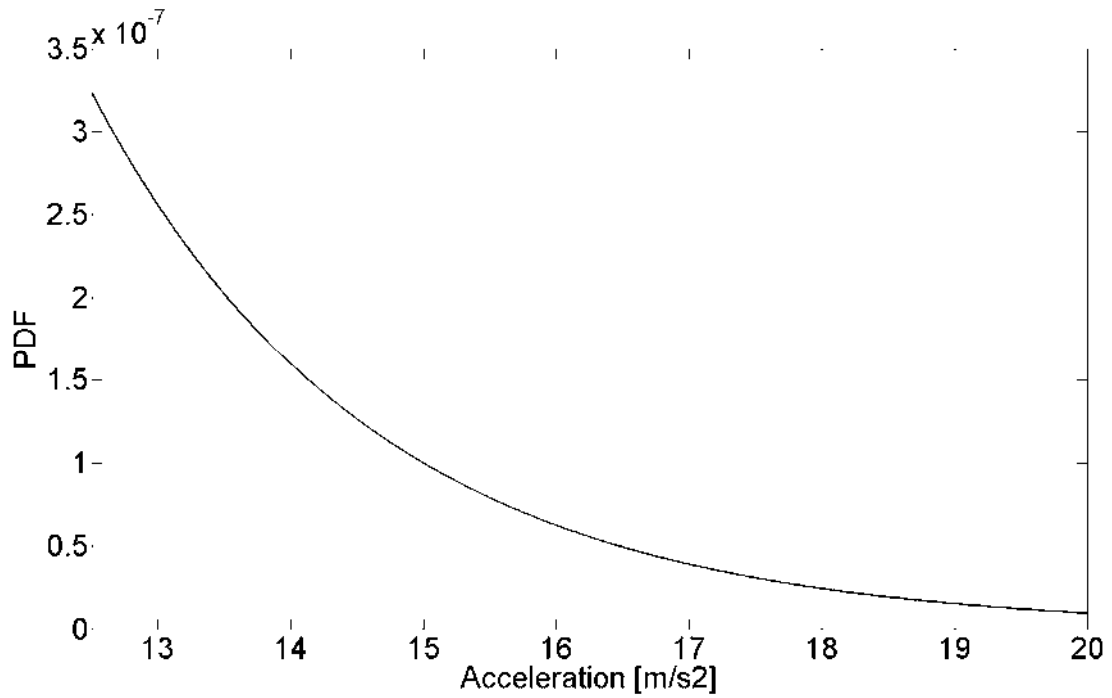Figure 16. Detail: PDF extended and truncated to 16m/s^2

Figure 17. Detail: PDF extended to 20m/s^2

Following these assumptions, the probability of failure has been computed for both the structural systems, plane and three-dimensional: Table 13 summarizes the total probabilities of failure for truncated and not truncated PDF. The 3-DOFS system presents a lower risk of failure due to the lower fragility feature; the truncated PDF also is a conservative assumptions for the total probability of failure.

Table 13. Failure probabilities

	P_f (16m/s^2 extended and truncated PDF)	P_f (20m/s^2 extended PDF)
3-DOFS	1.1642e-005	1.1799e-005
6-DOFS	1.6542e-005	1.6699e-005

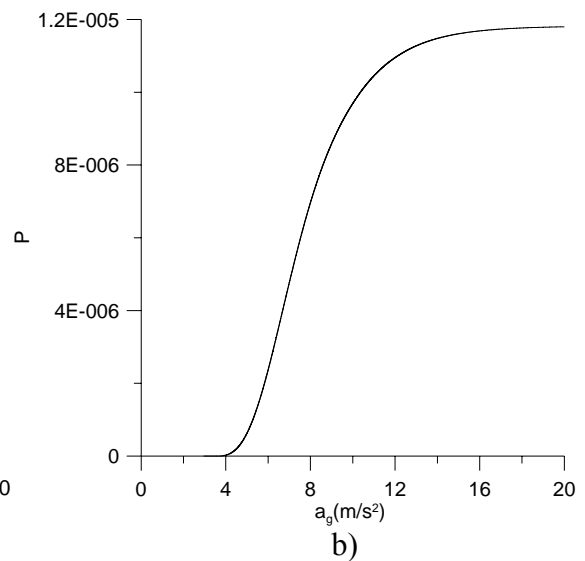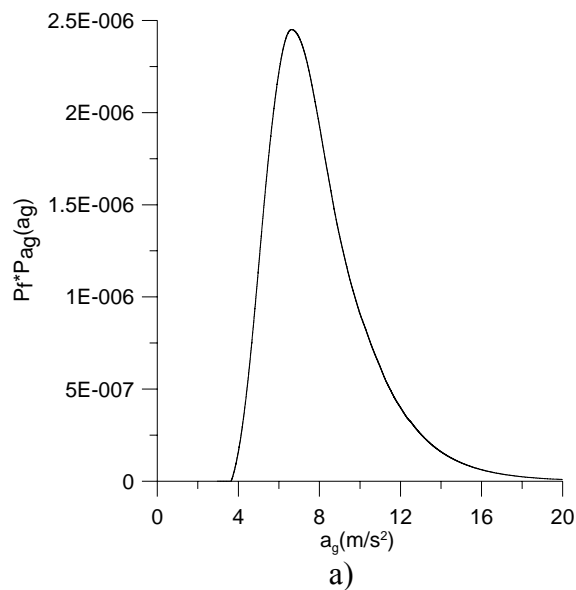a)   b)

Figure 18. 3-DOFS system: (a) integrand function (total probability theorem) with (b) probability of failure function
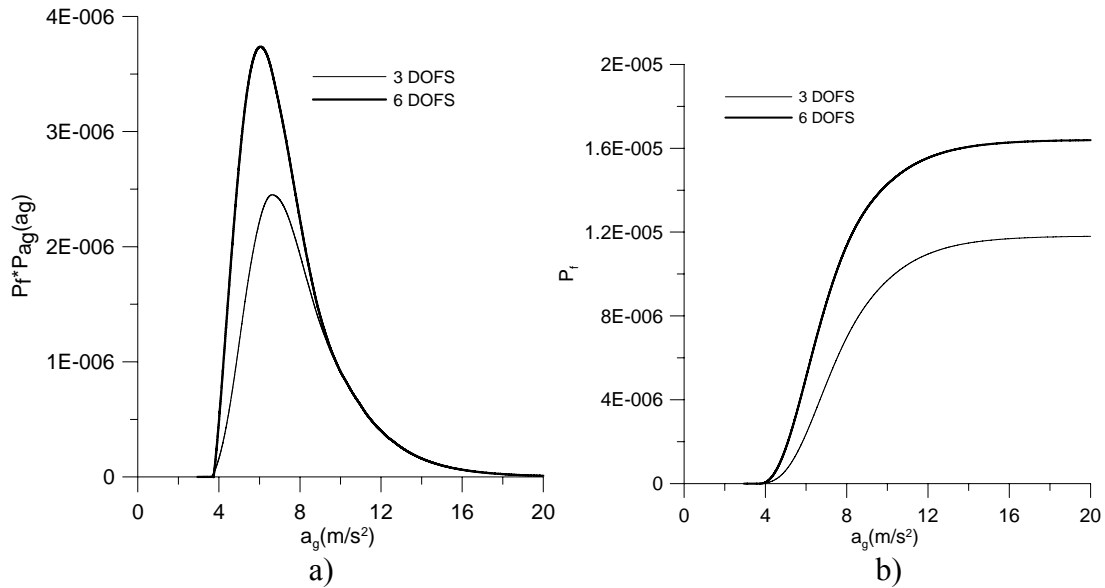
Figure 19. 6-DOFS system compared to 3-DOFS one: (a) integrand function (total probability theorem) with (b) probability of failure function

Figure 18a reports the integrand function computed by combining the not truncated, less conservative, hazard and the fragility function with the total probability theorem for the 3-DOFS option. Figure 18 b depicts the total failure probability. Similarly, Figures 19a and 19b shown the 6-DOFS model results; a comparison is also proposed.

13.   Conclusions

This study reports about the seismic risk computation of the isolated IRIS Reactor Building. When the base-isolation system based on HDRB is implemented, the acceleration values inside the building undergo a dramatic decrease. The isolation system itself becomes the weakest element in terms of seismic safety of the building.

MATLAB models of the Auxiliary Building are adopted with rigid body motion assumption by considering 3-and 6-DOFS approaches. The fragility analysis of the Reactor Building is then performed by consolidated analytical and numerical tools. The seismic risk is finally computed by considering an hazard function related to a medium seismicity site with two different extended PDFs (truncated and not truncated).

The proposed procedure, funded on consolidated numerical methods, results effective, though considering a limited number of random variables and a first tentative limit state domain for the devices.

14.   Recommendations and future developments

The limit state domain definition for delamination behaviour plays a significant role in the final risk assessment and its definition remains under development by this research group, studying similar approaches in literature on composite structures.

The laboratory activity is also a key point of the procedure and full scale assessment of the control devices seems mandatory for characterizing their mechanical behaviour in quasi-static

and dynamic conditions. The influence of the vertical force on the isolator horizontal behaviour seems also to be an remarkable aspect to be deepen.

Acknowledgements

References

[1]   Bianchi G., De Grandis S., Domaneschi M., Mantegazza D., Perotti F., "Seismic risk computation for the fixed base reactor building of the IRIS NPP", Technical Report ENEA NNFISS-LP-027, ENEA, September 28, 2010, Bologna, Italy.

[2]   De Grandis S., Domaneschi M., Perotti F., "A numerical procedure for computing the fragility of NPP components under random seismic excitation", Nuclear Engineering and Design, Volume 239, Issue 11, November 2009, Pages 2491-2499, ISSN 0029-5493, DOI: 10.1016/j.nucengdes.2009.06.027.

[3]   MATLAB R2008b, version 7.7.0.471 September 2008, The MathWorks inc.

[4]   Forni M., Poggianti A., Bianchi F., Forasassi G., Lo Frano R., Pugliese G., Perotti F., Corradi dell'Acqua L., Domaneschi M., Carelli M.D., Ahmed M.A., Maioli A., "Seismic Isolation of the IRIS Nuclear Plant", 2009 ASME Pressure Vessels and Piping Conference (PVP 2009), Prague; 2009; Code 80491. American Society of Mechanical Engineers, Pressure Vessels and Piping Division (Publication) PVP, Vol. 8, 2010, Pages 289-296. ISSN: 0277027X. ISBN: 978-079184371-0.

[5]   Grant D.N., Fenves G.L., Auricchio F. (May 2005), "Modelling and analysys of high-damping rubber bearings for the seismic protection of bridges", Research Report No. ROSE-2005/01, ROSE School, Collegio Alessandro Volta, Via Ferrata, 27100, Pavia, Italy.

[6]   Kikuchi M. and Aiken I.D. (1997), "An analytical hysteresis model for elastomeric seismic isolation bearings", Earthquake Engineering and Structural Dynamics, 26:215-231.

[7]   Hwang J.S., Wu J.D., Pan T.-C., Yang G. (2002), "A Mathematical Hysteretic Model for Elastomeric Isolation Bearings, Earthquake Engineering and Structural Dynamics, 31:771-789.

[8]   Tsai C.S., Chiang T.-C., Chen B.-J. And Lin S.-B. (2003), "An advanced analytical model for high damping rubber bearings", Earthquake Engineering and Structural Dynamics, 32:1373-1387.

[9]   Jankowski R. (2003), "Nonlinear Rate Dependent Model of High Damping Rubber Bearing", Bulletin of Earthquake Engineering, 1:397-403.

[10]   Abe M., Yoshida J., Fujino Y. (2004), "Multiaxial Behaviors of Laminated Rubber Bearings and Their Modeling. I: Experimental Study", ASCE Journal of Structural Engineering, 130(8): 1119-1132.

[11]   Abe M., Yoshida J., Fujino Y. (2004), "Multiaxial Behaviors of Laminated Rubber Bearings and Their Modeling. II: Modeling", ASCE Journal of Structural Engineering, 130(8): 1133-1144.

[12]   Ryan K.L., Kelly J.M., Chopra A. (2005), "Nonlinear Model for Lead-Rubber Bearings Including Axial-Load Effects", ASCE Journal of Structural Engineering, 131(12): 1270-1278.

[13]   Yamamoto S., Kikuchi M., Ueda M., Aiken I.D. (2009), "A mechanical model for elastomeric seismic isolation bearings including the influence of axial load", Earthquake Engineering and Structural Dynamics, 38:157-180.

[14]   Kikuchi M., Nakamura T., Aiken I.D. (2010), "Three-dimensional analysis for square seismic isolation bearings under large shear deformations and high axial loads", Earthquake Engineering and Structural Dynamics, 39:1513-1531.

[15]   Carelli, M.D., et al. (2004), "The design and safety features of the IRIS reactor", Nuclear Engineering and Design, 230: 151–167.

[16]   Perotti F. (2010), Lecture Notes of Structural Dynamics, Politecnico di Milano, Milano I.

[17]   ENEA Centro Ricerche Bologna, ReportXCESI-LP-001 (2010).

[18]   ENEA Centro Ricerche Bologna, Report XFIP-LP2-001 (2010).

[19]   Corradi dell'Acqua L., Domaneschi M., Guiducci C. (2009), "Assessing the reliability of seismic base isolators for innovative power plant proposals", 20th International Conference on Structural Mechanics in Reactor Technology (SMiRT20), Espoo Finland.

[20]   Der Kiureghian A. (2005), "Non-ergodicity and PEER's framework formula", Earth. Eng. Struct. Dyn., 34, P. 1643-1652.

[21]   Perotti F. et al. (2009), "Seismic Isolation of the IRIS NSSS Building", Proc. of SMiRT 20, Helsinki, Finland.

[22]   Faravelli L. (1989), "Response surface approach for reliability analysis", ASCE J. of Eng. Mech., 115, P. 2763-2781.

[23]   Casciati F. and Faravelli L. (1991), Fragility analysis of complex structural systems. Research Studies Press Ltd., Taunton, Somerset, England, P. 305-355.

[24]   Towashiraporn P. (2004), "Building seismic fragilities using response surface metamodels". Thesis in partial fullfillment of PhD deg. in Civ. and Env. Eng., Georgia Institute of Technology.

[25]   G.Bianchi, L.Corradi, M.Domaneschi, D.C.Mantegazza, F.Perotti, A.Ravez (2011), "LIMIT STATE DOMAIN OF HIGH DAMPING RUBBER BEARINGS IN SEISMIC ISOLATED NUCLEAR POWER PLANTS", *Submitted* to *SMIRT 21*, New Delhi, India.

[26]   USNRC 1.60 - Design Response Spectra For Seismic Design Of Nuclear Power Plant, Regulatory Guide, U.S. Atomic Energy Commission, December 1973.

[27]   Matlab (2008), The Language of Technical Computing, Version 7.7.0.471 – Theory Manual, (R2008b).

[28]   Rubinstein R.Y. (1981), "Simulation ad the Montecarlo Method", Wiley. ISBN 0-471-08917-6.